Chemical weathering and CO2 consumption in a multi-lithological karstic critical zone: Long term hydrochemical trends and isotopic survey

F. Ulloa-Cedamanos, Anne Probst, I. Moussa, J.-L. Probst

Chemical Geology 585 (2021) 120567

Contents lists available at ScienceDirect

Chemical Geology

journal homepage: www.elsevier.com/locate/chemgeo

Chemical weathering and CO_2 consumption in a multi-lithological karstic critical zone: Long term hydrochemical trends and isotopic survey

F. Ulloa-Cedamanos [a,b,c,*], A. Probst [a,b,c], I. Moussa [a], J.-L. Probst [a,b,c,*]

[a] Laboratoire écologie fonctionnelle et environnement, Université de Toulouse, CNRS, Auzeville Tolosane, 31326 Castanet Tolosan, France
[b] LTSER Zone Atelier Pyrénées-Garonne, CNRS, Université de Toulouse, 31326 Castanet Tolosan, France
[c] LTER Bassin versant du Baget, SNO Karst, IR OZCAR, CNRS, Université de Toulouse, 31326 Castanet Tolosan, France

ARTICLE INFO

Editor: Dr Oleg Pokrovsky

Keywords:
Carbonate dissolution
Weathering
$\delta^{13}C_{DIC}$ and $\delta^{34}S_{SO4}$
Mixing diagrams
Long-term hydrochemical survey
Seasonal patterns
Karst
Mountainous forested catchment

ABSTRACT

The chemical weathering (CW) of rocks at the Earth's surface plays a key role in the global carbon cycle along multiple pathways. Although karst systems are hotspot carbonated areas, they are not always monolithological. It is therefore challenging to estimate the CW of these complex areas. The interannual, seasonal, and spatial variations of CW rates and CO_2 consumption were investigated using a long-term hydrogeochemical database (1994–2019) from a mountainous karstic catchment in southwestern France (Baget Catchment). A geochemical and isotopic spatial sampling allowed the identification of the main mineral or lithological sources in the catchment, which controlled the water chemistry. The CW budget showed that the (Ca^{2+} + Mg^{2+}) fluxes originated from carbonate dissolution (1.14 mol·m^{-2}·yr^{-1} equivalent to 74%) and silicate weathering (18%) by carbonic acid solutions. Gypsum dissolution and carbonate weathering by sulphuric acid from pyrite oxidation contribute equally to 4%, although the former accounts for 66% of the dissolved sulphate fluxes. During a summer sampling survey, an innovative sulphur isotopic approach based on $\delta^{34}S_{SO4}$, allowed us to demonstrate that the ore-nature sulphuric acid drove 9.0% of total carbonate dissolution and represented only 16.8% of the dissolved sulphate stream fluxes. Hydrological conditions, temperature, vegetation, the epikarst (quasi-permanent shallow and discontinuous saturated layer under the soil), and the water dynamics were the key factors influencing the inter-annual and inter-seasonal variations of the CW rates and CO_2 consumption. In addition, the carbon isotopic signature evidenced geochemical processes such as CO_2 outgassing and calcite precipitation processes. The latter could remove up to 74% of HCO_3^- from streamwaters, depending on the hydrological conditions at the outlet between 2016 and 2019. Finally, this study highlights that CW rates and CO_2 consumption may vary over inter-annual and inter-seasonal scales, and spatially even for a small catchment. Furthermore, the global CO_2 consumption appears to be mainly driven by the runoff intensity in karst hydrosystems, where carbonate dissolution was found to consume 71% of the total weathering CO_2 uptake.

1. Introduction

The chemical weathering of crustal rocks is one of the major geological processes involved in climatic and chemical changes on the earth's surface (Spence and Telmer, 2005). Although this fundamental process is relatively well known, the identification and quantification of its spatial and temporal role in the carbon cycle remains a key question to be addressed (Berner and Kothavala, 2001).

Biogenic CO_2, the main natural actor, drives the chemical weathering of rocks, it is then transformed into dissolved inorganic carbon (DIC) and transported to the oceans by the river systems. Biogenic CO_2 results from the sequestration of atmospheric CO_2 by vegetation due to net primary production and subsequently from soil CO_2 released by the decomposition of organic matter and root respiration (Catalán et al., 2016; Clark and Fritz, 1997; Porcal et al., 2015). The two principal mineral groups consuming biogenic CO_2 are silicates and carbonates (Cao et al., 2019; Hartmann et al., 2009; Moquet et al., 2011). On million year scales (geological timescales), only the chemical weathering of silicates plays a major role in the carbon budget as a sink for atmospheric CO_2 (Curl, 2012; Dalai et al., 2002; Francois and Walker, 1992; Hartmann et al., 2009), since the precipitation of carbonates in the ocean counterbalances the dissolution of crustal carbonate rocks

* Corresponding authors at: Laboratoire écologie fonctionnelle et environnement, Université de Toulouse, CNRS, Auzeville Tolosane, 31326 Castanet Tolosan, France.
E-mail addresses: francesco.ulloacedamanos@toulouse-inp.fr (F. Ulloa-Cedamanos), jean-luc.probst@toulouse-inp.fr (J.-L. Probst).

https://doi.org/10.1016/j.chemgeo.2021.120567
Received 28 June 2021; Received in revised form 22 September 2021; Accepted 7 October 2021
Available online 13 October 2021

(Berner et al., 1983; Khadka et al., 2014). Nonetheless, over shorter timescales (less than ~100,000 years), carbonate dissolution contributes to drawing down carbon from the atmospheric reservoir due to its rapid dissolution kinetics (Cao et al., 2012; Daoxian, 1997).

Chemical weathering rates (CWR) and CO_2 fluxes can be driven by environmental parameters such as discharge (Amiotte Suchet and Probst, 1993; Bluth and Kump, 1994; Cao et al., 2019; Ding et al., 2017; Gislason et al., 2009; Moquet et al., 2016), temperature (Eiriksdottir et al., 2011; Gaillardet et al., 2019; Liu et al., 2013; White and Blum, 1995), vegetation (Berner, 1997; Calmels et al., 2014; Lenton and Britton, 2006; Lucas, 2001; Zhao et al., 2019), lithology (Amiotte Suchet et al., 2003; Amiotte Suchet and Probst, 1993, 1995; Viers et al., 2014), relief (Cao et al., 2019), and mechanical erosion (Hagedorn and Cartwright, 2009; Jacobson et al., 2003; West et al., 2005). Indeed, the above-mentioned environmental factors, which are interrelated with each other (Goudie and Viles, 2012) can act as catalysts or, conversely, as inhibitors of chemical weathering in a given catchment.

For several decades, many studies have estimated chemical weathering rates on a global scale (Amiotte Suchet, 1995; Amiotte Suchet et al., 2003; Amiotte Suchet and Probst, 1995; Berner et al., 1983; Gaillardet et al., 1999; Garrels and MacKenzie, 1972; Meybeck, 1987; Probst, 1992; Probst et al., 1997). These estimations have mainly been focused on large river basins in tropical/sub-tropical climates (Cao et al., 2019; Galy and France-Lanord, 1999; Gibbs, 1972; Mortatti and Probst, 2003; Stallard and Edmond, 1987; Stallard and Edmond, 1983), temperate climates (Amiotte Suchet and Probst, 1996; Amiotte Suchet and Probst, 1993; Donnini et al., 2016; Hagedorn and Cartwright, 2009; Jiang et al., 2018; Spence and Telmer, 2005; Zhang et al., 1995), and boreal/polar climates (Calmels et al., 2007; Huh et al., 1998; Millot et al., 2003). These assessments commonly rely on the composition of major elements in river waters to estimate the amount of dissolved matter and CO_2 consumption associated with rock weathering. A common obstacle with these calculations on a large scale is the discrimination and subsequent quantification of sulphur compounds in multi-lithological catchments. This difficulty lies for example in the multiple potential inputs of sulphate (SO_4^{2-}) in rivers. In addition, sulphide oxidation releases sulphuric acid which causes the weathering of other minerals such as carbonates, whose later deposition in the oceans represents a net source of CO_2 in the atmosphere (Dalai et al., 2002; Galy and France-Lanord, 1999; Hercod et al., 1998; Millot et al., 2003; Spence and Telmer, 2005). This challenge has been solved by combining the major element chemistry with sulphur isotope measurements (Burke et al., 2018; Calmels et al., 2007; Karim and Veizer, 2000; Kemeny et al., 2021; Spence and Telmer, 2005; Turchyn et al., 2013).

Globally, karst systems are hotspots of water resources and carbonate dissolution, and its associated CO_2 uptake (Binet et al., 2020; Gaillardet et al., 2019; Plan et al., 2009). These areas are sometimes complex and can consist of multiple lithologies whose influence has largely been constrained and quantified over the short term (Gao et al., 2009; Han and Liu, 2004; Liu and Han, 2020a; Qin et al., 2019; Zhong et al., 2017), but rather poorly in the long term (Macpherson and Sullivan, 2019). A better understanding of the annual and seasonal variations of the chemical weathering of rocks and the associated CO_2 consumption on the long-term, and of the contribution of the different sources in multi-lithological conditions, is thus needed. This is even more relevant in active-relief regions, since the climate-weathering feedback is stronger, turning them into the areas that are most sensitive to climatic changes (Maher and Chamberlain, 2014). Catchments of limited areas are suitable critical zones (CZ) to constrain these variations and they can be investigated more easily and in more detail, because the lithological strata, structures and vegetation conditions are less complex and better known than in larger basins (Marx et al., 2017).

Several processes regarding the carbon cycle can modify the intensity of carbonate dissolution rates and CO_2 consumption, such as vegetation respiration, the mineralisation of organic matter, soil microbial activity, and other bedrock weathering (Clark and Fritz, 1997; Deines, 1980; Li et al., 2010), but also CO_2 outgassing (Doctor et al., 2008; Liu and Han, 2020a), calcite precipitation (Li et al., 2008), and even anthropic activities such as dams (Wang et al., 2019, 2020). In addition, stable carbon isotopes ($\delta^{13}C$) allow identification of different carbon sources (Qin et al., 2019), thanks to its fractionation effects (Li et al., 2008) resulting from different biogeochemical processes. Moreover, both sulphur and carbon isotope signatures have been used successfully to trace natural and anthropogenic contributions to water chemistry (Jiang, 2012; Lang et al., 2011; Qibo et al., 2016). However, their coupling to constrain source contributions and geochemical in-stream processes (Li et al., 2008; Schulte et al., 2011; Spence and Telmer, 2005) in multi-lithological basins, have not been explored in detail.

The small and mountainous karstic Baget catchment in the French Pyrenees has been monitored through hydrochemical surveys since the 1980s, with a complete hydrogeochemical database having been obtained since 1994. Based on these long-term datasets and on a spatial geochemical field investigation, this paper aims to fill the above-mentioned gaps by: (i) evaluating the potential contribution of the different lithological end-members on a spatial and temporal scale using the chemical and isotopic composition of streamwaters; (ii) determining the weathering flux and the atmospheric/biogenic CO_2 consumption through carbonate and silicate weathering pathways and their inter-annual, seasonal, and spatial variations; (iii) identifying the key environmental parameters and the geochemical in-stream processes influencing the carbon cycle.

The supporting hypothesis was that: (i) among multi-lithological sources, carbonate dissolution by atmospheric/soil CO_2 remains the main source of the hydrogeochemical fingerprint in the quasi pristine karstic catchment, followed far behind by the weathering of less abundant bedrock (silicate and evaporitic rocks) or even minerals like pyrite, whose contributions vary according to hydrological conditions; (ii) among environmental factors, discharge is the main driver of the inter-annual and seasonal variations of the weathering rate; and (iii) in-stream processes such as calcite precipitation may modify the estimation of weathering CO_2 consumption.

2. Materials and methods

2.1. Description of the study area and sampling sites

The Baget catchment (hereafter, BC, Fig. 1) drains an area of 13.25 Km^2 in the central part of the French Pyrenees Mountains. This karstic catchment has a mean altitude of 950 m (498 to 1417 m.s.l.) with slopes of up to 60% in the central section of the basin (Mangin, 1975).

The BC is a karst landform developed on Jurassic and Cretaceous carbonate rocks, which have been exposed to metamorphism at high temperatures and low pressures (Choukroune, 1970). It lies on a mixed lithological area (Fig. 1). A relatively narrow band of crystalline limestone is bordered to the north and south by low-permeable rocks. Sulphide minerals are observed along the BC as minor or accessory phases within lithological units such as limestones (Mangin, 1975). Finely crystallised black dolomite outcrops in the north (Fig. 1). Upper Cretaceous formations appear as alternating clay-gravel conglomerates and, thin outcrops of Upper Triassic gypsum have also been reported by Debroas (2009). In the south, the limestones are in contact either with a breccia, or with a black clayey-sandstone pelite (Debroas and Souquet, 1972), which constitutes part of the black flysch.

The dominant land cover is the fir-beech forest which is mainly located on the north-facing slope. Forest cover is continuous and occupied 67% of the catchment in 2019. In the upper middle section, the south-facing flank is characterised by numerous pastures, which change to scrubland towards the downstream side (Mangin, 1975). The calcareous formations are covered by thin and discontinuous brown soils or rendzina soils, while podzolic soils have developed on detrital formations (Bakalowicz, 1979). Anthropogenic pressure is very low with

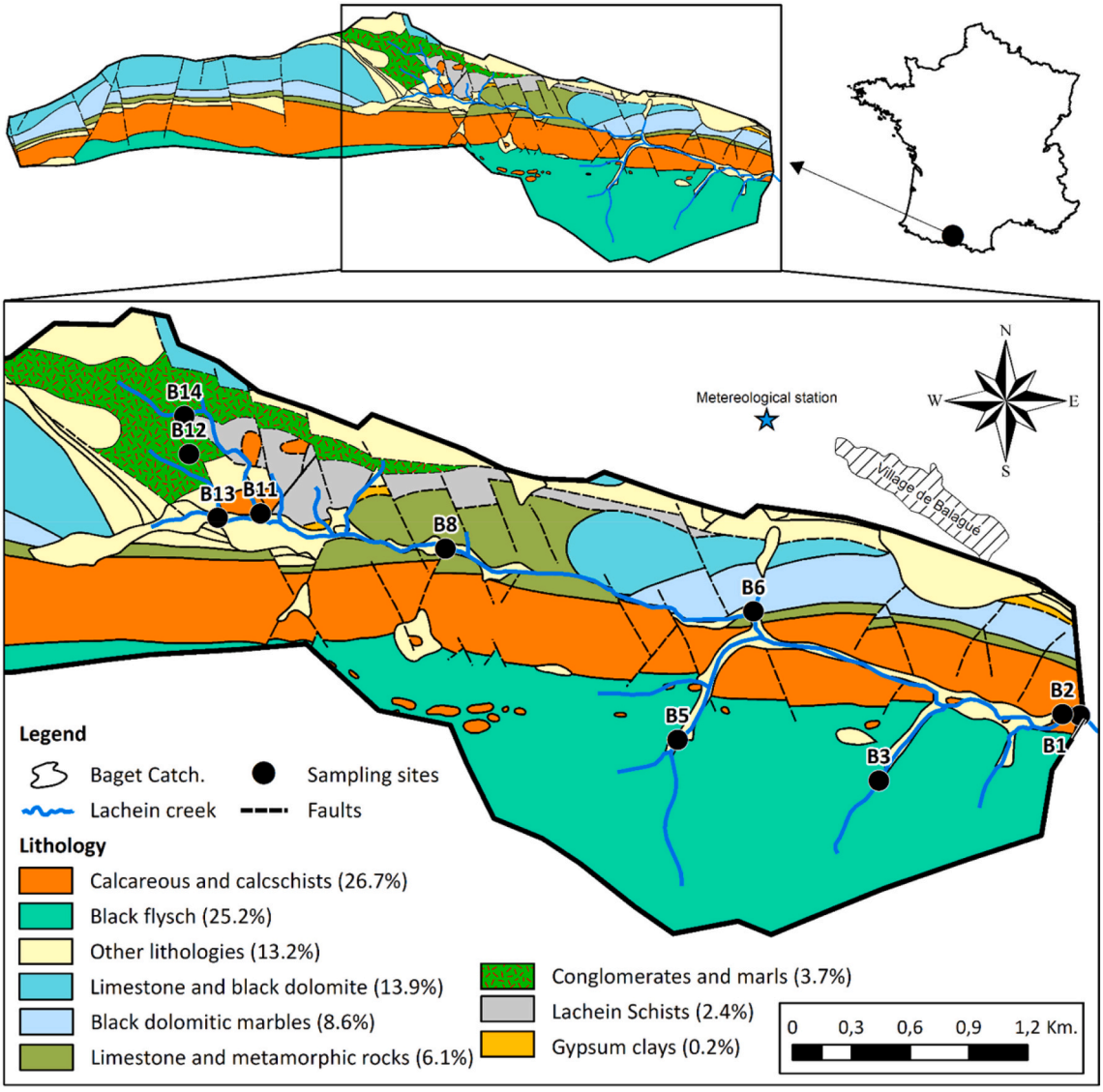

Fig. 1. Location of the Baget karstic catchment with the main lithology formations (1/50000, modified from BRGM-Info-Terre and Ulloa-Cedamanos et al., 2020) and the sampling stations (B1 to B14). Sampling stations B4, B7, B9 and B10 were not sampled due to the absence of runoff during the sampling period and are not displayed on the figure.

only very few human inhabitants and some crib barns (Bakalowicz, 1979). Some grasslands occupy the lower part close to the outlet on the south-facing slope.

The BC is subject to an Atlantic oceanic climate with a mountain influence resulting in a bimodal rainfall regime. The mean annual stream discharge at the catchment outlet (B1) is 0.48 $m^3 \cdot s^{-1}$, corresponding to a specific discharge of 36 $L \cdot s^{-1} \cdot km^{-2}$. Around 50% of the total discharge occurs between December and March (Ulloa-Cedamanos et al., 2020). BC is a responsive hydro-system with quick infiltration and a fast transit time between the recharge area and discharge at the outlet (Mangin, 1975; Sivelle et al., 2019; Ulloa-Cedamanos et al., 2021). The memory effect, which represents the inertia of the system, is estimated at 110 h based on hourly discharge series (Mangin, 1984).

The long-term hydrochemical survey (period 1994–2019) was performed at the catchment outlet (site B1, Fig. 1) and allowed the evaluation of the temporal patterns of interannual and seasonal variations (Ulloa-Cedamanos et al., 2020). In addition, spatial water sampling was carried out during low water conditions at the end of the summer in 2019 (12-13/09/2019, B1 to B14 sites, Fig. 1) to avoid the dilution of streamwater by meteoric water and to obtain the hydrochemical signature of each lithology (Ulloa-Cedamanos et al., 2020). During that period, the stream discharge was stable with a mean value of 0.08 $m^3 \cdot s^{-1}$, which is within the interannual average (from 1994 to 2019) of daily discharge for August (0.10 ± 0.05 $m^3 \cdot s^{-1}$) and September (0.11 ± 0.09 $m^3 \cdot s^{-1}$).

The target sites were chosen as follows, in order to determine the potential weathering fingerprint contribution of the main lithological formations to the streamwater chemistry (Fig. 1): (i) the whole basin with the sites B1 (Lachein creek at the outlet) and B2 (the spring called "Las Hountas", which can feed up to 100% of the discharge in B1 during summer); (ii) the black flysch (sites B3 and B5), the dolomitic formations (site B6), and the conglomerates (sites B12 and B14); (iii) the upper middle area of the Lachein creek (site B8); (iv) the outcrop area of the conglomerates, but also the Lachein schists together with the carbonate formation (site B11); and (v) the upper part of the BC (Lachein creek at site B13).

2.2. Sampling and analysis

2.2.1. Hydrochemical measurements

The hydrochemical monitoring was performed at the catchment outlet (B1, Fig. 1). Streamwater samples were collected (i) every week by the CNRS laboratory of Moulis from 1978 to 2006 (Binet et al., 2020), (ii) every six months by BRGM Midi-Pyrénées (ADES database, 2021) from 2007 to 2014, and (iii) fortnightly and more often during flood events by the Laboratoire écologie fonctionnelle et environnement from 2014 until present (for more details on the hydrochemical database until 2018, see Ulloa-Cedamanos et al., 2020). During this latter period and the 2019 summer spatial campaign, streamwater temperature, pH, specific conductivity, and dissolved oxygen were also measured in the field using a portable multi-parameter (WTW probe, Xylem Analytics Germany Sales GmbH & Co., Weilheim, Germany). The pH electrode of the WTW probe was calibrated with three buffer solutions (at pH 4, 7, and 10) before each sampling. Water samples were collected in a clean 1 L HDPE bottle and filtered in the laboratory through Millipore 0.22 μm cellulose nitrate membranes within 48 h after sampling. Only the filtrate aliquots for cation analysis were acidified with three drops of 16 N HNO_3. Water samples were stored at 4 °C in the dark from the time of collection to the time of analysis. Alkalinity was measured by the standard titration method with HCl 0.02 N, using a Metrohm titrator (716 DMS Titrino, Metrohm, Riverview, Florida, USA). The major dissolved cations (Ca^{2+},Mg^{2+}, Na^{+}, K^{+}) were determined by inductively coupled plasma optical emission spectrometer (ICP-OES; Iris Intrepid II XLD, Thermo Electron, Thermo Fisher Scientific, Waltham, MA, USA), while the major dissolved anions (SO_4^{2-},Cl^{-}, NO_3^{-}) were measured by ion chromatography (Dionex apparatus ICS 5000+, Thermo Fisher Scientific, Waltham, MA, USA). The accuracy of the analyses was controlled using blanks and two Certified Reference Materials (ION-96.4 and ION SUPER 05) depending on the range of ion concentrations. Instrumental detection limits for major ions ranged between 0.2 and 65 $\mu mol \cdot L^{-1}$.

Regarding the quality assurance (QA) and the quality control (QC), the data set was too long to have a QA/QC procedure over the entire period from 1978 until 2019. Concerning the QA, the protocols for the sampling, filtration, pre-treatment, and storage of the streamwater before analysis were controlled during the entire period. In relation to the QC, all the methods of analysis were controlled following French (NF), European (EN), and international (ISO) standards. The Net Inorganic Charge Balance ($NICB = 200 \times (|TZ^{+}|-|TZ^{-}|)/(|TZ^{+}| + |TZ^{-}|)$) between the sum of cations (TZ^{+}) and the sum of anions (TZ^{-}) (considered both in $meq \cdot L^{-1}$) was always within a ± 10% range for all species indicating that the water composition was well described by the measured major dissolved species. Moreover, for several decades, the physico-chemical analysis platform of the Laboratoire écologie fonctionnelle et environnement has participated each year in the ICP-Water Intercomparison protocol lead by the Norwegian Institute for Water Research (NIVA), which follows a QA/QC procedure.

2.2.2. Isotopic analyses

The carbon isotope analyses of dissolved inorganic carbon ($\delta^{13}C_{DIC}$) were performed on stream waters collected once a month at the outlet of BC (B1, Fig. 1) from 2016 onwards and during the spatial sampling (09/2019). Samples were collected using 10 mL glass vials, which had previously been filtered using a 0.2 μm filter membrane. Before filling, the vial was rinsed three times with an aliquot of the filtrate. Then, the sample was stored in darkness at 5 °C before analysis. Additionally, in March 2019, water was sampled at: (i) sites B1, B2, B3, and B6 (Fig. 1) following the same collection procedure described above to later analyse $\delta^{13}C_{DIC}$ and (ii) site B1, filtering this water sample through a 0.7 μm glass microfiber filter (GFF) that had previously been pyrolysed. The remaining particulate matter in the dry filter was decarbonated to analyse the particulate organic carbon isotope composition ($\delta^{13}C_{POC}$). Isotopic analyses were performed using an isotope ratio mass spectrometer (CF-IRMS, Isoprime100, Cheadle Hulme, UK) with a continuous flow system (Elementar/Isoprime, Multiflow-Geo) at the Laboratoire écologie fonctionnelle et environnement (SHIVA isotopic platform). Precision for the method was better than $\pm 0.2‰_{vpdb}$ for all samples based on replicate analyses of samples and standards.

Sulphur isotopes of dissolved sulphates ($\delta^{34}S_{SO4}$) were only determined on samples collected during the spatial sampling under base flow conditions (09/2019). The water samples were collected in clean 1 L bottles, filtered using a 0.22 μm filter membrane and acidified to pH 3 by addition of HCl 36 N Suprapur. Then, 6 mL of 1 M $BaCl_2$ solution was added dropwise to precipitate $BaSO_4$ for collection on a 0.2 μm polycarbonate membrane and storage in glass capsules. All the capsules were kept at 5 °C in the dark from the time of collection to the time of analysis by an elemental analyser interfaced to an Isotope Ratio Mass Spectrometry (EA-IRMS) at Iso-Analytical Limited, Crewe, UK (http://www.iso-analytical.co.uk). The $\delta^{34}S_{SO4}$ values were determined and reported relative to Canyon Diablo Troilite (CDT), with a precision of $\pm 0.1‰_{CDT}$ by comparison to replicate sample analyses and to reference materials calibrated and traceable to International Standards (NBS-127 and IAEA-S-1).

2.3. Data treatment

2.3.1. Statistical analysis

All calculations were computed at the scale of the hydrological year (H.Y., from October to September). For simplicity, only the second year of each period will be mentioned, for example the period from October 2018 to September 2019 will be indicated as the hydrological year 2019. The mean concentrations were discharge-weighted. Statistical data treatments like the hierarchical cluster analyses and the graphical methods such as Stiff (1951) and Piper diagrams (Hamilton, 2018; Piper, 1944) were performed using R (CRAN, the Comprehensive R Archive Network).

2.3.2. Partial pressure of carbon dioxide and calcite saturation index calculations

The partial pressure of carbon dioxide (pCO_2) and saturation index of calcite ($SI_{calcite}$) were computed with the PHREEQC program (Version 3.7; database wateq4f, Parkhurst and Appelo, 1999) using the data of major ion concentrations, pH, and water temperature measured in situ as initial conditions.

2.3.3. Flux calculation method

The annual fluxes (F_{annual}) of the different major elements, corresponding to each hydrological year are the result of the sum of all the fluxes (n) calculated between two sampling intervals (i to i + 1) using the discharge-weighted mean concentration (C_j) and the water volume (V_j) for each time period (i to i + 1) as follows:

$$C_j = \frac{\sum_i^{i+1} C_i \, x \, Q_i}{\sum_i^{i+1} Q_i}, \quad (1)$$

$$F_{annual} = \sum_i^n \left(C_j \, x \, V_j\right), \quad (2)$$

with C_i and C_{i+1} representing the concentrations at time periods i and i + 1, respectively; Q_i and Q_{i+1} being the discharge at time i and i + 1, respectively; and V_j is the volume of water flow between i and i + 1.

2.4. Discrimination of major ions in streamwaters

The sources of dissolved major elements at each sampling point include the atmospheric and biogenic inputs, and the different mineral/rock weathering contributions (Meybeck, 1986; Spence and Telmer, 2005). A geochemical model called MEGA (Amiotte Suchet, 1995) was developed to calculate the potential contribution of these inputs to the water chemistry and the associated CO_2 consumption (Amiotte Suchet and Probst, 1996). This model is based on the stoichiometry of the

chemical reactions after the correction of atmospheric and biogenic inputs (Probst et al., 1997). The methodology used to determine each end-member contribution, i.e., the MEGA model, is explained in detail in Supplementary Information A.

3. Results

3.1. Chemical and isotopic compositions of streamwaters

All the parameters and the major ion concentrations measured in streamwater samples are listed in Table 1 for the long-term monitoring at the outlet of BC (site B1, expressed as mean interannual value) and for the spatial sampling campaign. A similarity was expected between all values at the outlet (site B1) and the perennial spring Hountas (site B2), since site B2 is the main contributor to the Lachein creek at site B1, especially during the period of low water flow in summer.

Streamwaters were circumneutral to alkaline. The pH measured during the spatial sampling campaign at sites B1 and B2 was similar to the mean interannual pH value at the outlet (B1), whereas the other sampling sites exhibited higher pH values (between 8.2 and 8.3). The exception is site B12, which is a small spring located in the upper part of the basin (Fig. 1). A similar pattern was observed for water temperature. The interannual mean value of TDS at the outlet was in the same order of magnitude as half of the sites, but it was lower than the following sites: B5 < B13 < B6 < B12 << B8.

The mean interannual concentrations of the different ions (Fig. 1, Fig. 2) and their respective contribution to the total anionic and cationic charges (Supplementary Information B Fig. B1) indicated that Ca^{2+}, followed far below by Mg^{2+}, were the dominant cations, and HCO_3^-, followed also by far by SO_4^{2-}, were the dominant anions at the outlet (site B1).

During the spatial sampling, a similar pattern was observed for cations, except at site B6 where Mg^{2+} and K^+ had the highest contributions (31% and 2%, respectively), and at B3 and B5, where Na^+ slightly exceeded Mg^{2+}. The mean interannual Ca^{2+}/Mg^{2+} molar ratio was 8 at B1, but it varied strongly among the sites between 2 (site B6) and 27 (site B5) for the spatial sampling. For the anions, a similar pattern was also observed during the sampling campaign, with the exclusion of site B8 where HCO_3^- represented only 34% of the total anions, while SO_4^{2-} represented 65% (Fig. 1, Supplementary Information B Fig. B1), whereas it ranged between 4% and 16% for the other sites. The HCO_3^-/SO_4^{2-} molar ratio oscillated widely from 0.5 (B8) to 27 (B14). The contributions of Cl^- and NO_3^- concentrations were very low (<3%, except Cl at B6), NO_3^- being relatively higher at site B3, as well in the lower part of the basin. Silica ranged from 45 μmol·L^{-1} (B1 and B2) to 148 μmol·L^{-1} (B3). The $H_4SiO_4/(Ca^{2+}+Mg^{2+})$ molar ratio was higher at the sites B3 and B5 draining silicate-bedrocks (0.09 and 0.07, respectively) compared with the other sites (between 0.01 and 0.04) (Table 1).

3.2. Clustering analysis on major elements in streamwaters

The Stiff diagram (Fig. 2A) compares graphically the chemical patterns at the different sites by plotting jointly the concentrations of dissolved major elements during the spatial sampling (Table 1). It helped distinguish sites particularly affected by distinct lithological formations (Hem, 1986; Hounslow, 1995). Based on the diagram shapes and the location of the sites on the lithological map (Fig. 1), we made an *a priori* classification of the sites (Fig. 2A). The Hierarchical Clustering Analysis (HCA, Fig. 2B) was used to augment the Stiff diagram results by integrating more chemical variables such as dissolved silica (H_4SiO_4) and the pH of the water (Table 1). HCA classifies a large number of individuals, reducing them to a small number of streamwater groups with similar lithological origins (Cloutier et al., 2008). The number of clusters depended on the threshold for the linkage distance. The threshold was fixed at 1 so that six clusters (C1 to C6) could be distinguished (Fig. 2B) based on the streamwater's chemical composition. These clusters relate to the bedrocks over which the streams are draining: (C1) B8 for evaporitic rocks (gypsum); (C2) B3 and B5 for silicate rocks; (C3) B1 and B2 for a mixing of lithologies; (C4) B11 and B14 for conglomerates and marls; (C5) B6 for dolomitic rocks; and (C6) B12 and B13 for calcite-bearing rocks.

3.3. Temporal and spatial variations of the different sources

The average potential contributions of each lithological formation as well as the atmospheric and biogenic inputs to the riverine dissolved loads were assessed using the geochemical discrimination detailed in Supplementary Information A. These potential contributions were

Table 1
Main physico-chemical and isotope characteristics of the waters draining the Baget catchment. "Interannual Mean B1" is the average value for the period 1994–2006 plus 2016–2019 (up to 707 samples). The other codes (sites B1 to B14) represented the sites sampled during the spatial sampling in September 2019 (see Fig. 1). The units are L·s^{-1} (Q, discharge), °C (T°, water temperature), μS·cm^{-1} (Cond, conductivity), meq·L^{-1} (major elements), mmol·L^{-1} (H_4SiO_4), mg·L^{-1} (TDS), ‰$_{VPDB}$ ($\delta^{13}C_{DIC}$) and ‰$_{CDT}$ ($\delta^{34}S_{SO4}$). (–) means no data. The mean pH (calculated from mean H^+), concentrations and TDS were discharge-weighted.

	Interannual mean B1 (± σ)	Summer 2019									
		B1	B2	B3	B5	B6	B8	B11	B12	B13	B14
Q	465 ± 734	78	61	0.15	0.64	0.35	1.38	0.24	0.02	0.002	0.84
T°	10.3 ± 0.17	10.5	10.4	12.2	12.5	13.7	11.1	14.2	13.6	13.8	12.7
pH	7.7 ± 0.21	7.8	7.7	8.3	8.2	8.3	8.3	8.3	7.7	8.3	8.2
Cond	317 ± 19	365	364	343	347	401	835	327	525	488	336
Ca^{2+}	3.02 ± 0.17	2.99	3.02	3.16	3.26	2.71	7.22	2.76	3.88	3.44	2.98
Mg^{2+}	0.36 ± 0.06	0.44	0.44	0.13	0.12	1.31	1.01	0.35	0.51	0.61	0.25
Na^+	0.05 ± 0.01	0.04	0.04	0.14	0.13	0.10	0.07	0.05	0.04	0.04	0.06
K^+	0.01 ± 0.00	0.01	0.01	0.01	0.00	0.09	0.04	0.01	0.01	0.02	0.01
HCO_3^-	2.99 ± 0.20	2.79	3.00	2.84	3.14	3.97	3.08	3.19	4.25	4.08	3.18
SO_4^{2-}	0.34 ± 0.13	0.53	0.54	0.47	0.56	0.29	5.94	0.27	0.48	0.17	0.12
Cl^-	0.05 ± 0.01	0.04	0.05	0.06	0.05	0.13	0.05	0.04	0.03	0.04	0.03
NO_3^-	0.03 ± 0.02	0.00	0.04	0.09	0.03	0.09	0.02	0.01	0.01	0.01	0.01
H_4SiO_4	0.04 ± 0.01	0.05	0.05	0.15	0.11	0.07	0.08	0.06	0.06	0.07	0.05
TDS [a]	273 ± 15	269	286	286	303	349	644	277	375	344	271
pCO_2	$10^{-2.5}$	$10^{-2.7}$	$10^{-2.5}$	$10^{-3.2}$	$10^{-3.0}$	$10^{-3.0}$	$10^{-3.1}$	$10^{-3.1}$	$10^{-2.4}$	$10^{-3.0}$	$10^{-3.0}$
SIc	0.1	0.2	0.1	0.7	0.6	0.8	0.9	0.7	0.4	0.9	0.6
$\delta^{13}C_{DIC}$	−12.3 ± 0.4 [b]	−12.4 [c]	- [c]	−11.0 [c]	−9.6	−8.8 [c]	−7.9	−8.8	−3.9	−10.9	−5.2
$\delta^{34}S_{SO4}$	–	11.3	11.4	−5.5	−8.1	4.3	13.3	−5.4	−4.1	1.1	−2.2

[a] TDS is the total dissolved solids (TDS = $Ca^{2+} + Mg^{2+} + Na^+ + K^+ + HCO_3^- + SO_4^{2-} + Cl^- + NO_3^- + H_4SiO_4$, protons and ammonium being neglectable).
[b] Mean interannual value was calculated based on the data available from October 2016 to September 2019.
[c] The $\delta^{13}C_{DIC}$ signature during the spatial sampling in March 2019 were −12.8 (B1), −11.7 (B2), −9.9 (B3) and −9.2 (B6).

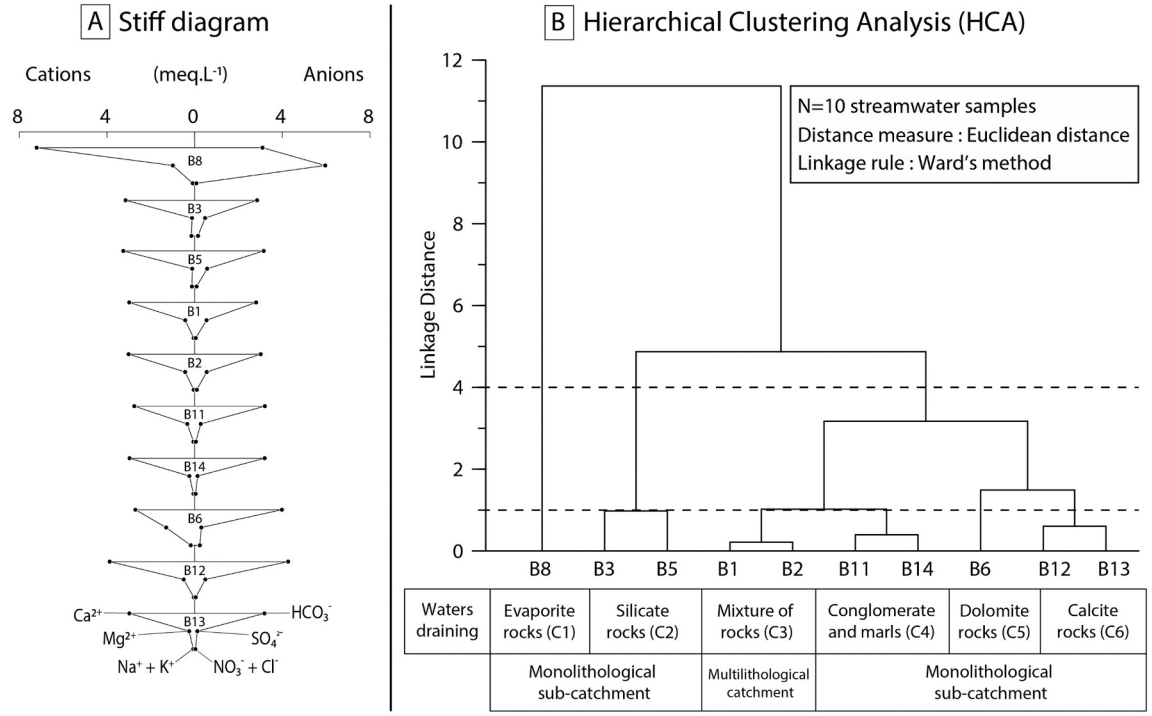

Fig. 2. Comparison of the chemical patterns using the Stiff diagram (A) and hierarchical clustering analysis (B) of the streamwater chemical composition of the different sites for the spatial sampling campaign. The drainage bedrocks are mentioned for each cluster of sites.

calculated at the catchment outlet (B1) for each year (annual average, Fig. 3A) and each month (interannual monthly average, Fig. 3B) during the period 1994–2019 (avoiding 2007–2016 due to sparse data), and for each site (B1 to B14) during the spatial sampling (Fig. 3C).

The highest fluxes of all inputs occurred in periods with the largest amounts of precipitation and discharge. The inputs from the atmosphere (Atm, 2.9%) and from the leaching of organic matter (Bio, 0.7%) represented 3.6% of the interannual mean TDS at the outlet (B1) (Fig. 3A, B). The limited atmospheric input contribution is consistent with the low concentrations measured in open field precipitation (mean TDS = 4 ± 1 mg L^{-1}). Indeed, Mg^{2+}, K^{+}, SO_4^{2-}, NO_3^{-}, and NH_4^{+} concentrations were very low (mean concentration of these major dissolved species < 6 µmol·L^{-1}) (Ulloa-Cedamanos et al., 2021). Concerning the spatial sampling, results showed a quite homogenous variation of the low atmospheric input contribution to TDS (Fig. 3C). The contribution of the leaching of fir–beech forest (Bio) was lower than 1%, except for sites B3 and B6. Due to the absence of a forest at site B6, unlike site B3, we considered a slight pollution (group "Ant" in red, Fig. 3C) representing only 3.2% of TDS. This anthropogenic input was minimal at site B6 and was not observed elsewhere. Furthermore, the overall catchment is considered as pristine (Bakalowicz, 1979; Mangin, 1975; Ulloa-Cedamanos et al., 2020). Abnormally high potassium values in B6, which together with nitrate are closely related to some agricultural/livestock activities (Busico et al., 2020; Chetelat et al., 2008; Lechuga-Crespo et al., 2020; Xu and Liu, 2007), reinforced this hypothesis.

The mean interannual TDS potential contributions of mineral/rock weathering in B1 followed this pattern: pyrite oxidation (1% of TDS) < carbonate dissolution by H_2SO_4 (3%) ≈ gypsum dissolution (3%) << silicate weathering by H_2CO_3 (16%) << carbonate dissolution by H_2CO_3 (73%).

Regarding interannual variations at B1 (Fig. 3A), the major elements coming from pyrite oxidation and from gypsum dissolution were low (up to 1.5% and from 1.6% to 4.9% of TDS, respectively). Carbonate dissolution by ore-nature sulphuric acid reached up to 4.2% of TDS. Inputs from silicate weathering showed a slight oscillation between 3.4% (4.0 g·s^{-1} of TDS) and 5.7% (7.2 g·s^{-1}), while the TDS potential contribution of alkalinity released by the associated CO_2 consumption varied from 8.2% to 15.0%. The major TDS inputs, due to carbonate dissolution (including only 50% of the total alkalinity produced), ranged from 44.9% (30.9 g·s^{-1}) to 50.7% (60.9 g·s^{-1}) according to the year. The TDS potential contribution of alkalinity derived from the atmospheric/soil CO_2 (50% of the total alkalinity produced by carbonate dissolution) varied from 25.2% to 29.8% of TDS.

With respect to seasonal variations (Fig. 3B), the highest fluxes were observed during winter, mainly in February, while the lowest ones occurred during summer, predominantly in August. However, the TDS potential contributions (in %) followed different variation patterns according to the lithological formation and the mineral. The lowest TDS potential contributions from pyrite oxidation (1.0%), gypsum dissolution (2.3%), and silicate hydrolysis (13.6%) were observed in May and June, while that of carbonate dissolution (79.0%) exhibited the highest values. Conversely, carbonate dissolution presented its lowest TDS potential contribution (70.0%) from July to September, while pyrite oxidation (1.4%), gypsum dissolution (8.4%), and silicate weathering (18.0%) exhibited highest TDS potential contributions. Moreover, carbonate dissolution by sulphuric acid was on average lower than 3.8% of TDS but in July it reached up to 8.4%. Furthermore, the TDS potential contribution of carbonate dissolution had increased again by October, and it was counterbalanced by a relative decrease of the TDS potential contributions supplied by the weathering of the other lithological formations.

Concerning the spatial sampling, the discrimination (Fig. 3C) was consistent with the results of the statistical analysis (Sub-section 3.2). There were remarkable differences in chemical characteristics between the outlet (site B1) and its tributaries. The pyrite oxidation (Pyr) and the consequent carbonate dissolution by sulphuric acid was non-negligible for sites B3 and B5, whereas gypsum dissolution (Gyp) represented 55% of TDS at site B8 while at the other sites, it was always less than 11%. Silicate weathering and associated CO_2 consumption were less of 29% for all sites, except for B3 (63%) and B5 (56%). Carbonate dissolution and associated CO_2 consumption were the most relevant contributors for the other sites: B11 (64% of the total TDS stream flux) < B6

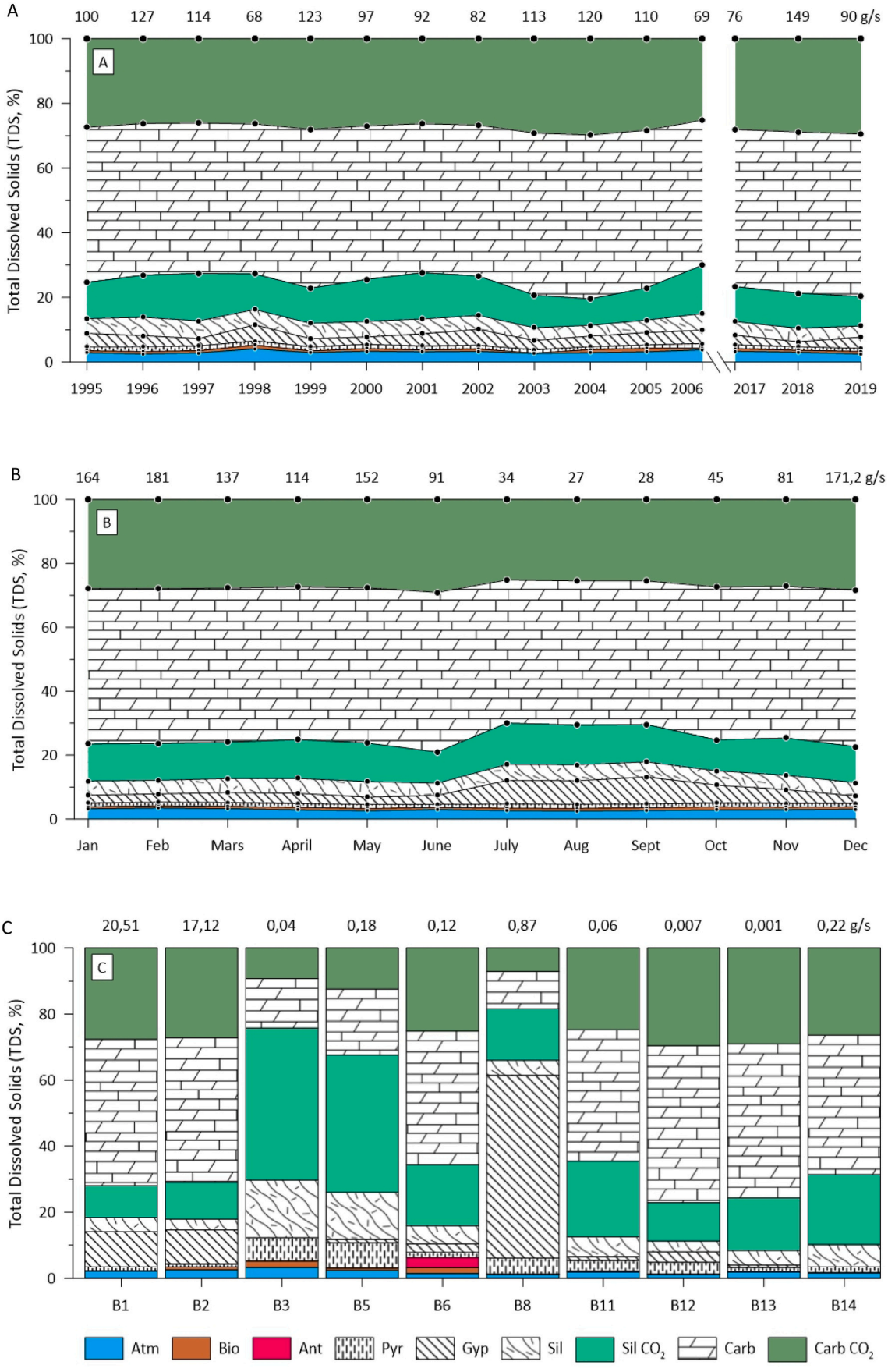

(caption on next page)

Fig. 3. Potential Contribution (%) of the different rock/mineral weathering to the total TDS stream fluxes. (A) interannual variations for the period 1994 to 2006 plus 2016 to 2019, (B) interannual monthly average for the same period and (C) instantaneous values for the spatial sampling (sites B1 to B14) in summer 2019. For each year, month or site, the TDS stream fluxes ($g{\cdot}s^{-1}$) is given in the upper part of each figure at the top of each column. The TDS potential contribution is composed by atmospheric inputs (Atm), leaching of organic matter (Bio), anthropogenic (Ant), weathering of sulphide minerals (Pyr), gypsum dissolution (Gyp), silicates mineral hydrolysis (Sil), carbonate dissolution (Carb) and the CO_2 consumption associated to carbonate dissolution (Carb CO_2) and silicate weathering (Sil CO_2) released as part of the alkalinity. "Carb" includes the carbonate dissolution by H_2CO_3 and H_2SO_4.

(66%) < B14 (69%) < B2 (71%) < B1 (72%) < B13 (76%) < B12 (77%).

3.4. Carbon ($\delta^{13}C_{DIC}$) and sulphur ($\delta^{34}S_{SO4}$) isotopic signatures in streamwaters

According to the pH range in BC streamwaters, HCO_3^- (bicarbonate) was the dominant species of DIC (Schulte et al., 2011), and therefore $\delta^{13}C_{DIC}$ was rather similar to $\delta^{13}C_{HCO3-}$. At the outlet of BC (site B1), the $\delta^{13}C_{DIC}$ signature in streamwaters based on monthly monitoring between 2016 and 2019, ranged between −13.2 and − 11.7‰$_{VPDB}$ (Table 1). No significant correlation was found between HCO_3^- concentration and $\delta^{13}C_{DIC}$. The $\delta^{13}C_{DIC}$ values in the BC were in the same range of values measured in river water and spring water draining carbonate-rich basins like the Auradé catchment in Gascogne, France (between −15.2 and −10.7‰$_{VPDB}$; Brunet et al., 2011) or the Beipanjiang River basin (mean value of −10.5 and −8.3‰$_{VPDB}$; Li et al., 2008) or river water draining the silicate-rich catchments like the Strengbach in the Vosges mountains in France (yearly average of −11.8‰$_{VPDB}$; Amiotte-Suchet et al., 1999), or the Nyong in Cameroon (−21.8 to −11.3‰$_{VPDB}$; Brunet et al., 2009) which can be impacted by important CO_2 degassing. Nevertheless, they were lower than those in the Rhône River basin mainly dominated by carbonate rocks and detrital sediments (between −10 and − 5‰$_{VPDB}$; Aucour et al., 1999), the Patagonian rivers (between −10 and − 3.8‰$_{VPDB}$; Brunet et al., 2005), or the multilithological Ganga-Brahmaputra River system (between −12 and 0‰$_{VPDB}$; Galy and France-Lanord, 1999). Conversely, the $\delta^{13}C_{DIC}$ in BC was higher than the spring and piezometer waters from the Strengbach silicate-rich catchment (mean values of −20.3 and −18.9‰$_{VPDB}$, respectively; Amiotte-Suchet et al., 1999) and the rivers draining the basalt-rich Deccan Traps (between −20.7 and −8.5‰$_{VPDB}$; Das et al., 2005). Besides, compared to the mean inter-annual variations (Table 1), the spatial sampling showed a marked variation of $\delta^{13}C_{DIC}$, ranging from −12.4‰$_{VPDB}$ (B1) to −3.9‰$_{VPDB}$ (B12).

The dissolved sulphate concentrations ranged from 0.12 to 0.56 $meq{\cdot}L^{-1}$, except for site B8 (5.94 $meq{\cdot}L^{-1}$). The $\delta^{34}S_{SO4}$ values varied widely from −8.1 (site B5) to +13.3‰$_{CDT}$ (site B8).

4. Discussion

4.1. Sources of dissolved elements and weathering processes: geochemical and isotopic constraints

According to the geochemical discrimination (MEGA model), as expected, the major source contributing to streamwater chemistry was the chemical weathering of rocks, which is generally reflective of the imprint of the weathering product in the solutes of the river (Gaillardet et al., 1999; Lechuga-Crespo et al., 2020; Liu and Han, 2020b; Moon et al., 2007), whereas the atmospheric and the biogenic inputs were the lowest ones, accounting for only 2.9% and 0.7% of the mean interannual TDS, respectively. Despite the multilithology (presence of silicates, gypsum and pyrites), the impact of carbonate dissolution predominated at the outlet (72.6 ± 3.5% of the mean interannual TDS; Fig. 3), even if only around 66.5% of surface area in BC was occupied by carbonate terrains (Fig. 1). Their mere presence in the catchment leads to a high proportion of their dissolution in the water chemistry (Blum et al., 1998; Liu et al., 2018), which is consequently stable due to the buffer capacity of carbonates. This is in agreement with previous studies in BC (Bakalowicz, 1979; Binet et al., 2020). The lesser fingerprint of silicate weathering by carbonic acid (15.9%) is the consequence of low silicate mineral solubility compared to carbonates. Sulphate represented only 10% of the total anion concentration despite being the second major anion in BC (Table 1). The very low fingerprint of gypsum dissolution (3.2%) and pyrite oxidation (1.2%) which represent the main sulphate sources, is due to the very low relative abundance of these minerals within BC.

The hydrological and lithological conditions play an important role in these respective contributions, as was revealed by the results obtained during the spatial campaign. At this low water flow period, most of the sampled sites evidenced the dominance of carbonate dissolution. Nevertheless at sites B3 and B5, silicate weathering by carbonic acid contributed the most to the streamwater chemistry (67% and 61% of TDS, respectively), followed far behind by carbonate dissolution by carbonic acid (20% and 26% of TDS, respectively). In addition, gypsum dissolution governed the streamwater chemistry at site B8 (60% of TDS). Our investigations underline that the type of bedrock and its distribution in the catchment play an important role on the chemical composition of stream waters even in carbonate-dominated karst systems. It cannot be neglected with reference to water level conditions (Meybeck, 2003; Viers et al., 2014 and references therein), but these potential weathering contributions can be minimised downstream by a simple dilution from a pure carbonated source, as it is the case in the Lachein creek (Cf. B1 outlet influenced by B2 source).

The geochemical approach using major dissolved elements was not completely constrained to assess the weathering processes and the understanding and quantification of the potential contributions to the weathering products. It remains challenging for example to discriminate the influence of sulphide oxidation and evaporite dissolution to riverine sulphate and to stream TDS. The large range of $\delta^{34}S_{SO4}$ and of $\delta^{13}C_{DIC}$ values observed for the different tributaries illustrate the complexity of the hydrochemistry in BC. An original approach combining sulphate isotope constrain to the geochemical discrimination, was thus developed (Supplementary Information C).

The geochemical potential contributions of these end members (sulphide oxidation and evaporite dissolution) were thus estimated using a novel mixing diagram based on the relationship between $\delta^{34}S_{SO4}$ (Supplementary Information C Eq. C1-C4) and R_{SO4}, the molar ratio $SO_4^{2-}/(Ca^{2+}+Mg^{2+})$, measured during the spatial sampling (Fig. 4). For all sites, the values calculated from this mixing diagram are similar to those calculated using the geochemical discrimination (Supplementary Information B Fig. B4). The most important differences between the two approaches occurred in B8, a gypsum-rich site. This difference revealed the strong sensitivity of the proposed mixing diagram of $\delta^{34}S_{SO4}$ to detect and better restrict the potential contribution at sites where sulphate was the dominant anion. This difference was based on the complexity of estimating the R_{pyr} and R_{sil} ratios in site B8 (geochemical discrimination), since the potential contribution of gypsum represented 60.9%, while its outcrop only covered 0.3% of the surface of the whole basin. For the rest of the sites, the difference was always less than ±6% (Supplementary Information B Fig. B4). For instance at the outlet of BC, the sulphuric acid released by pyrite oxidation drove 5.0% (geochemical discrimination) to 9.0% (mixing diagram) of total carbonate dissolution and represented 12.9% to 16.8% of the dissolved sulphate stream fluxes, respectively.

The two main sources of DIC are the carbonate mineral dissolution and the atmospheric/soil CO_2 consumed by carbonate dissolution and silicate hydrolysis. Carbon isotopes can also help to better constrain the

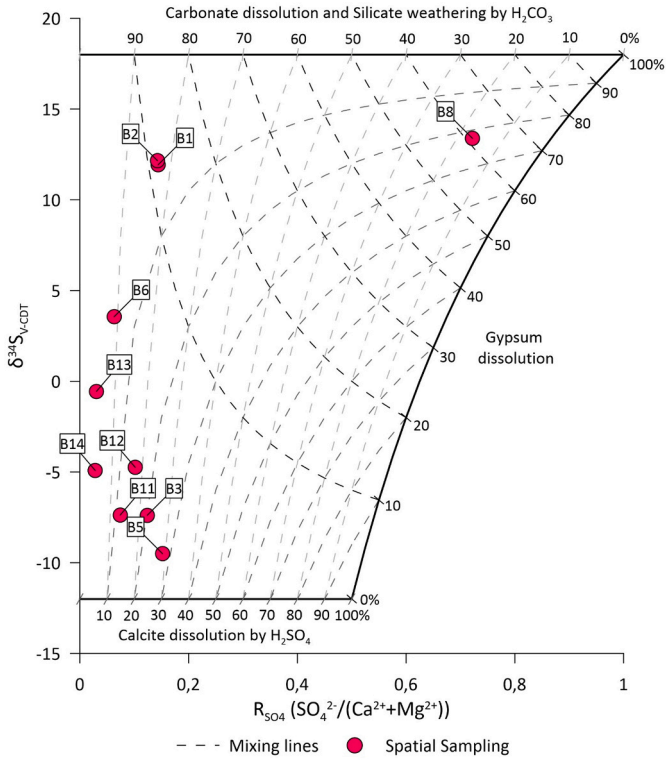

Fig. 4. Relationship between $\delta^{34}S_{SO4}$ and R_{SO4} ($SO_4^{2-}/Mg^{2+}+Ca^{2+}$) for the water samples collected during the spatial sampling at the different sites (B1 to B14). The end-member compositions as described in the text are shown to represent the position of each site on the different mixing lines (dashed lines).

geochemical approach. Carbonate rocks, mainly formed by the precipitation of carbonates in the ocean, have shown typical marine values of $\delta^{13}C$ close to 0‰$_{VPDB}$ since the end of the Proterozoic (Veizer et al., 1999). The isotopic signature of biogenic CO_2 in soils rely directly on the dominant metabolism pathway, resulting mainly in C3 plants (estimated average isotopic composition of −26‰$_{VPDB}$) and C4 plants (−12‰$_{VPDB}$) (Deines, 1980). The $\delta^{13}C$ signature of Particulate Organic Carbon (POC) measured in March 2019 at site B1 (−28.6‰$_{VPDB}$) can be associated with the presence of C3 plants (from −30‰ to −24‰; Clark and Fritz, 1997) as the dominant species in the catchment. Afterwards, this carbon is subjected to fractionation depending on the temperature and the rate of CO_2 diffusion (Aucour et al., 1999; Deines et al., 1974).

Therefore, we have defined the following three $\delta^{13}C_{DIC}$ weathering end-members based on the stoichiometry of mineral weathering (Supplementary Information B Table B1 Eq. B5-B12) and on the average isotopic compositions of the different sources (Doctor et al., 2008; Mook, 2000):

(i) First end member (CW): the dissolution of one mole of carbonate by carbonic acid (Supplementary Information B Table B1 Eq. B9-B10, exponent "CW") requires one mole of dissolved soil CO_2 ($\delta^{13}C = -19$‰$_{VPDB}$, Amiotte-Suchet et al., 1999) and one mole of carbonate ($\delta^{13}C = 2 \pm 3.5$‰$_{VPDB}$), releasing DIC with a $\delta^{13}C_{DIC}{}^{CW}$ signature around -8.5 ± 1.75‰$_{VPDB}$;

(ii) Second end-member (SW): the dissolution of silicate minerals by carbonic acid Supplementary Information B Table B1 Eq. B5-B8, exponent "SW") only needs dissolved soil CO_2, producing DIC with a $\delta^{13}C_{DIC}{}^{SW}$ signature around −19‰$_{VPDB}$;

(iii) Third end member (pyr): the carbonate dissolution by sulphuric acid (Supplementary Information B Table B1 Eq. B11-B12, exponent "pyr") producing a DIC isotopic signature $\delta^{13}C_{DIC}{}^{pyr}$ close to that of carbonate, 2 ± 3.5‰$_{VPDB}$.

After identifying each end member, a mass balance can be applied to calculate an expected $\delta^{13}C_{DIC}$ signature (Spence and Telmer, 2005) in streamwaters using the results obtained from the hydrogeochemical discrimination (MEGA model results) for DIC origins:

$$\delta^{13}C_{DIC}^{exp} = \%DIC^{pyr} x\, \delta^{13}C_{DIC}{}^{pyr} + \%DIC^{SW} x\, \delta^{13}C_{DIC}{}^{SW} + \%DIC^{CW} x\, \delta^{13}C_{DIC}{}^{CW} \quad (3)$$

The relationship between $\delta^{13}C_{DIC}$ and R_{SO4} (Fig. 5A) indicated a slight enrichment in $\delta^{13}C_{DIC}$ between July and October at the outlet, even if the $\delta^{13}C_{DIC}$ of most samples had a relatively narrow range. This suggested a relative increase of the contribution of carbonate dissolution by sulphuric acid during the summer, which was consistent with the observed relative increase in sulphide oxidation contribution (Fig. 3B). The hypothesis of a CO_2 release was discarded since soil and water pCO_2 values are the highest during this season (Mangin, 1975; Ulloa-Cedamanos et al., 2020), showing only calcite precipitation (Fig. 5B). Moreover, the ratio R_{SO4} increased significantly from the wet season to the dry season, mostly due to the relative increase of gypsum dissolution contribution and, to a lesser extent, of sulphide oxidation contribution (Fig. 3B; Fig. 7B). The influence of gypsum dissolution is also observed in site B8, where R_{SO4} tends towards 1 (0.72, Fig. 5A). Moreover, the spatial sampling allowed two biogeochemical processes to be highlighted: the CO_2 outgassing and the calcite precipitation which tend to increase or decrease the $\delta^{13}C_{DIC}$ signature in streamwaters, respectively. This leads to the positioning of the samples along the vertical axis, outside the mixing diagram (Fig. 5A). The mixing diagram therefore illustrated the different processes but could not be used to estimate their influence. Instead, a theoretical $\delta^{13}C_{DIC}$ isotopic signature in streamwater ($\delta^{13}C$ MEGA) was calculated using the results of the geochemical discrimination concerning the DIC contributions of the different lithological sources (Eq. 3) and their respective average $\delta^{13}C_{DIC}$ signatures. Then, these theoretical $\delta^{13}C_{DIC}$ values were compared with the $\delta^{13}C_{DIC}$ measured in the streamwater samples (Table 1; Fig. 5B).

Some possible explanations for the difference between the measured and calculated $\delta^{13}C_{DIC}$ are described below:

(1) The carbonate dissolution by sulphuric acid can be overestimated at the outlet (site B1). In this case, the R_{sil} and R_{pyr} ratios should be underestimated and overestimated, respectively. However, these ratios were determined for small rivers draining monolithological catchments in France (Meybeck, 1986) and were validated by spatial sampling data as well as by comparison with the results given by the $\delta^{34}S_{SO4}$ mixing diagram (Fig. 4). Indeed, the contribution of pyrite oxidation is already restricted, representing only 1.2% of the mean interannual TDS. Furthermore, during the spatial sampling, the contribution of carbonate dissolution by sulphuric acid represented only 3.3% (MEGA) and 5.7% ($\delta^{34}S_{SO4}$ mixing diagram) of streamwater TDS from the chemical weathering of rocks at the outlet (Fig. 4).

(2) The $\delta^{13}C_{DIC}$ can be shifted by the outgassing of CO_2 from the river waters to the atmosphere. The groundwater and soil influx discharged into river water always have a remarkably high pCO_2 level compared with that in the atmosphere (Boano et al., 2014; Deirmendjian and Abril, 2018; Doctor et al., 2008). Hence, this CO_2 concentration gradient between river water and atmosphere would cause a strong diffusion accompanied with a rapid CO_2 outgassing (Richey et al., 2002), which could lead to a higher $\delta^{13}C_{DIC}$ signature (Liu and Han, 2020a). This statement matches clearly with the surface water collected at the different sites (from B3 to B12, Fig. 1) during the spatial sampling, where the streamwater pCO_2 have dropped down approaching the atmospheric pCO_2 (Fig. 5B).

(3) Secondary calcite precipitation may also be a possible mechanism for $\delta^{13}C_{DIC}$ shifting (Li et al., 2008) toward lower values. Indeed, the position of the two spring waters (sites B2 and B13) and the

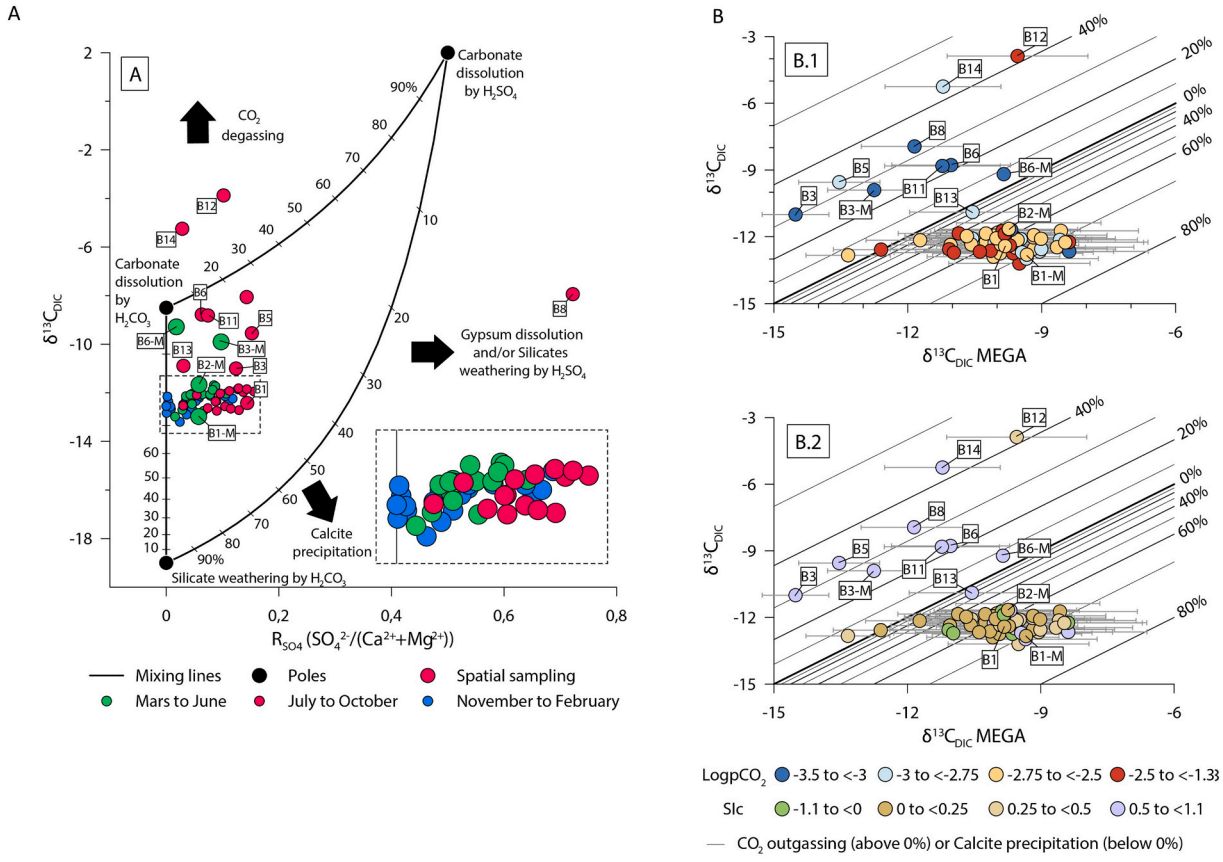

Fig. 5. (A) Relationships between $\delta^{13}C_{DIC}$ and R_{SO4} ($SO_4^{2-}/(Ca^{2+}+Mg^{2+})$), showing the influences of the different processes. End-member compositions as described in the text are shown to illustrate that most of the waters are distributed along a mixing line. The black arrows indicate possible reasons for the deviations from these mixing lines. Values from 10 to 90 over the mixing lines represent the potential contribution percentage of each end member for each dot. Nomenclature of 4 sites sampled in March 2019 ends with "-M" (B) Relationships between the $\delta^{13}C_{DIC}$ signature measured in streamwaters ($\delta^{13}C_{DIC}$) and the $\delta^{13}C_{DIC}$ value calculated using the geochemical discrimination ($\delta^{13}C_{DIC}$ MEGA): (B1) according to the pCO_2 and (B.2) to the Saturation Index of calcite (SIc). The uncertainties (horizontal grey lines) are due to the isotopic signature of carbonate rocks. Straight black lines represent theoretical processes of CO_2 outgassing (above theoretical line 0%) and carbonate precipitation (under theoretical line 0%), according to the end-members compositions represented in Fig. 5.A (for further details, see Supplementary Information B Table B4).

outlet (B1) which is mainly fed by the spring waters of site B2, are deviated from the line 1:1 (Fig. 5B). This could thus be explained by secondary carbonate precipitation which could remove up to 74% of HCO_3^-, according to hydrological conditions and/or to the end-member isotopic signatures (Fig. 5A).

4.2. *Chemical weathering budget and CO_2 consumption fluxes*

The weathering rates calculated in this study are slightly different to previous calculations for this multilithological catchment. For example, the mean interannual flux of Ca + Mg due to carbonate dissolution by carbonic acid and by strong acid was calculated as 1.14 mol·m^{-2}·yr^{-1} and 0.06 mol·m^{-2}·yr^{-1}, respectively. Meanwhile, Binet et al. (2020) suggested a higher flux of Ca + Mg released from carbonate dissolution by carbonic acid (1.30 mol·m^{-2}·yr^{-1}) and by strong acid (0.39 mol·m^{-2}·yr^{-1}). The main difference resides in that our estimations also consider inputs from gypsum dissolution (Ca + Mg flux of 0.06 mol·m^{-2}·yr^{-1}) and Ca-Mg silicate weathering (Ca + Mg flux of 0.27 mol·m^{-2}·yr^{-1}).

A total of 34% of the sulphate was attributed to sulphide oxidation which was lower but in the same order of magnitude as recent estimates for global average rivers (e.g., 46%; Burke et al., 2018). However, the sulphuric acid produced by sulphide oxidation drives only 6.8% of carbonate dissolution. Even though sulphide oxidation tends to occur much more rapidly than silicate weathering (Singer and Stumm, 1970), the limited presence of sulphide-rich deposits in BC led that the total DIC produced by sulphuric acid consumed from carbonate dissolution being five times lower than the DIC produced by Ca-Mg silicate hydrolysis in the BC.

The contributions of carbonate dissolution and silicate hydrolysis to the total CO_2 consumption by weathering (1595 × 10^3 mol·km^{-2}·yr^{-1}) represent 71% and 29%, respectively. This CO_2 uptake was significantly higher than previous values estimated by Binet et al. (2020) for BC and for karstic carbonate catchments in France such as Lez, Farfal, Fontaine de Vaucluse, and Val d'Orléans. Unlike in this study, Binet et al. (2020) considered carbonate dissolution as the single source of Ca^{2+}, Mg^{2+}, and HCO_3^-, neglecting the contribution of silicate hydrolysis and evaporite dissolution to water chemistry. The BC CO_2 flux was also higher than the average CO_2 flux consumed by carbonate outcrops worldwide (478 × 10^3 mol·km^{-2}·yr^{-1}; Amiotte Suchet et al., 2003). Moreover, there are obvious climatic regional difference in the weathering rate and corresponding carbon sink capacity of river basins. Nevertheless, the runoff intensity remains the main driver of carbonate dissolution and CO_2 consumption during the formation of karst hydrosystems. As seen in Fig. 6, there is a significant relationship between the weathering CO_2 fluxes and the runoff intensity for different carbonate-rich river basins worldwide under different morphologic and bio-climatic regions. For instance, the total CO_2 consumption flux in BC is significantly higher than that in the Alps (Donnini et al., 2016), in the Himalayan Mountains such as the Si-Kiang river (Amiotte Suchet et al., 2003) and, in Chinese

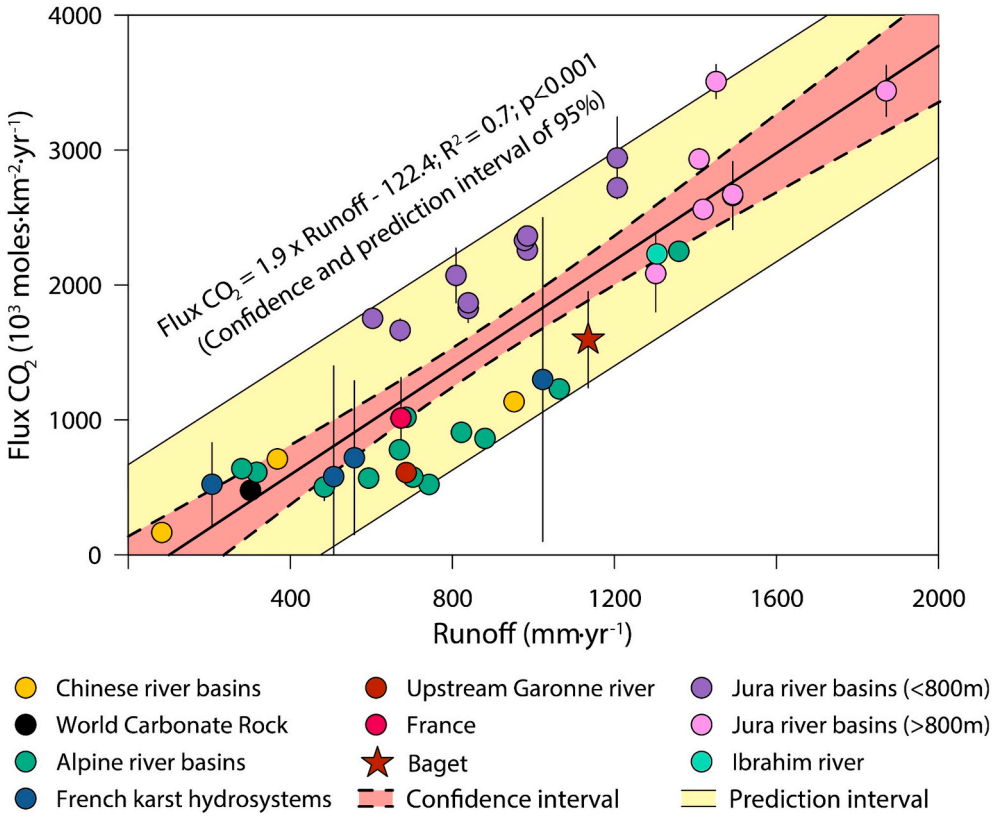

Fig. 6. Relationship between the specific fluxes of CO_2 consumed by chemical weathering (in 10^3 mol·Km^{-2}·yr^{-1}) and the mean runoff intensity (in mm·yr^{-1}) for different carbonate hydrosystems in the world and for the world carbonate areas (for references and further details, see Supplementary Information B Table B5).

karst hydrosystems (Liu and Zhao, 2000) (Fig. 6). Meanwhile, the CO_2 consumption fluxes estimated in this study were lower than those calculated for the Ibrahim River in Lebanese mountains (Assaker, 2016) or the Jura mountains in the North East of France (Calmels et al., 2014).

The CO_2 consumption flux in the BC corresponded, on average, to 117 and 11 t·km^{-2}·yr^{-1} of carbonate and silicate weathering rates, respectively. For carbonate rocks (density of 2.7 g·cm^{-3}), this specific weathering flux was equivalent to a mean denudation rate of about 43.4 mm·kyr^{-1}, accounting for less than half of the carbonate being dissolved in the Jura Mountains (Calmels et al., 2014); it was, however, much higher than in other catchments in Asia (Chetelat et al., 2008; Galy and France-Lanord, 1999; Xu and Liu, 2007). According to Viers et al. (2014), the chemical denudation rate varies between 15 and 100 mm·kyr^{-1} for carbonates worldwide.

4.3. Factors controlling bedrock weathering rates

The amount of draining water as reflected by the stream discharge plays a key role in the mineral weathering processes and consequently, over the TDS exportation by the river (Cao et al., 2019). This primary control is evidenced by the strong positive dependence of all TDS fluxes on the stream discharge (Fig. 3; Fig. 7). Indeed, BC is a responsive karstic catchment with a rapid fluid transit time (Mangin, 1975; Sivelle et al., 2019; Ulloa-Cedamanos et al., 2021). Consequently, the dissolved elements in streamwater mainly originate from lithological formations with high dissolution kinetics, such as carbonates. Conversely, it was observed in BC that the sudden increase in discharge due to rainwater and surface runoff can lead to the dilution processes (Ulloa-Cedamanos et al., 2020) of elemental concentrations. This was the case during the wet period for the waters draining the silicate and gypsum lithologies, from which TDS contribution was decreased. On the contrary, the rapid dissolution rate of carbonates enables their greater contribution as a fingerprint to streamwater chemistry, even in periods of heavy rainfall characterised by short times of water-rock interaction (Fig. 3B, Fig. 7B; Alkattan et al., 1998; Tipper et al., 2006; Liu et al., 2018). As discharge increases, the carbonate predominance is also enhanced by an enlargement of the reactive mineral surface area, promoting mineral weathering (Clow and Mast, 2010; Qin et al., 2020). In addition, the variations in stream discharge affect not only the TDS fluxes, but also play a key role in modifying the relative contribution of some rock weathering sources to streamwater chemistry, between high and low flow periods (Fig. 3B). This process can be illustrated in summer when the water level decreases, and more soil and rock surface areas would be exposed to oxidising conditions, enabling for a higher relative contribution of sulphide oxidation (Spence and Telmer, 2005). This is supported by a relatively increased contribution of pyrite oxidation releasing sulphuric acid, up to 8.4% of the total carbonate dissolution during the low water period in July and August (i.e., an increase of 48% compared to the lowest estimated contribution from pyrite oxidation, Fig. 3B; Fig. 7B). Also, some Lachein tributaries/sections dry out completely during the low water period in summer, leading to an increased relative contribution of the permanent draining water areas. This explains the increased contribution to stream TDS (from 2.7% in June to 7.3% in July) of the gypsum dissolution (Fig. 3B; Fig. 7B). However, these processes can be highlighted only during the seasonal variations and cannot be observed through the inter-annual variations. At the inter-annual time scale, only primary controls of the discharge over the TDS fluxes can be observed from year to year (Fig. 3A; Fig. 7A).

In the 1980's, acid atmospheric deposition has been shown to influence the weathering of rocks, soils, and the water quality, even in remote mountainous areas such as the Strengbach catchment (Vosges Mountains; Probst et al., 1992) or in the Baget catchment (Pyrenees Mountains; Binet et al., 2020). However, in the last decades, acid atmospheric deposition has been strongly reduced (Pierret et al., 2019; Schöpp et al.,

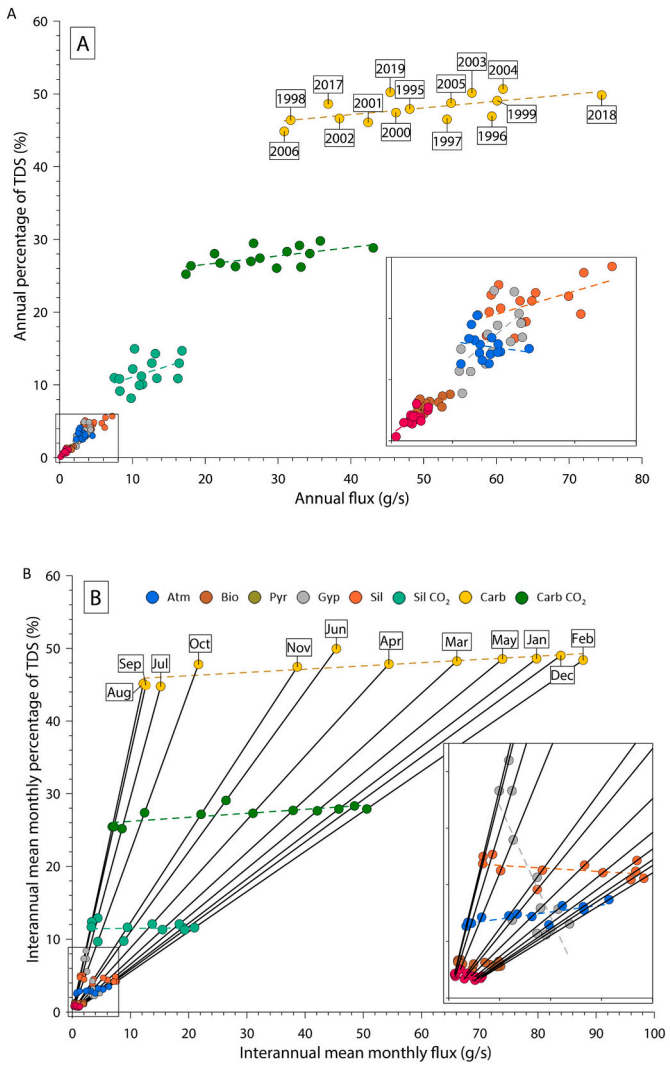

Fig. 7. Relationships between TDS flux contribution (%) and TDS fluxes (g/s) for the different sources during the period 1994 to 2006 plus 2016 to 2019: (A) for mean annual values and (B) for interannual mean monthly values. The different sources contributing to stream TDS are: atmospheric inputs (Atm), organic matter leaching (Bio), sulphide mineral oxidation (Pyr), gypsum dissolution (Gyp), silicate mineral hydrolysis (Sil), carbonate dissolution (Carb) and the atmospheric/soil CO_2 consumption associated to the dissolution of carbonates (Carb CO_2) and the weathering of silicates (Sil CO_2). The anthropogenic (Ant) contribution is negligible at the outlet.

2003). In the BC, Binet et al. (2020) showed that the decreasing trend in sulphate deposition has an influence on the decreasing pattern observed for Ca + Mg concentrations from the seventies. Nevertheless, in recent decades, the contribution of atmospheric sulphuric acid deposition to carbonate dissolution has remained very low as attested by the neutral precipitation with very low sulphate concentrations (< 8 μeq·L^{-1} from October 2019 to present).

Temperature is another pivotal controlling factor on rock weathering rates. In temperate and mountainous climates such as the study site in the Pyrenees Mountains, it behaves inversely with discharge. From a strictly mineralogical point of view, temperature increase promotes the dissolution reactions of minerals, except for calcite whose solubility decreases with rising temperatures (Plummer and Busenberg, 1982). The observed increase in air temperature coupled with the vegetation cover are the main factors associated with seasonal changes of biogenic pCO_2, which is involved in carbonate dissolution and silicate weathering (Supplementary Information B Table B1 Eq. B5-B10). Zeng et al. (2021) suggested that the role of biogenic pCO_2 in carbonate dissolution is critical in low-temperature zones (<15 °C). This biogenic role decreases at high erosion rates in high altitude areas, which are associated with a stronger effect of climate (temperature and runoff) on weathering fluxes (Maher and Chamberlain, 2014; West, 2012). Although the BC is located in the Pyrenees, the average elevation is rather low (950 m) with a mainly forested land cover, which enhances the biological role over rock weathering.

The epikarst plays also an important role on carbonate dissolution and stream TDS fluxes. This compartment allows: (i) an active exchange between the subsurface flow and base flow (Li et al., 2010), (ii) a CO_2 accumulation effect (Peyraube et al., 2013), and, (iii) a concentration effect in the stored water during summer, a period of high soil mineralisation and consequently, a high weathering/dissolution of rock by high pCO_2 levels. These loaded epikarst waters (old water) should be released with the first heavy rainfalls in autumn (Aquilina et al., 2006; Bakalowicz, 2012; Kirchner, 2003). This "piston effect" of waters from the epikarst influenced by these factors could be revealed by a sudden increase of Ca^{2+}, Mg^{2+}, and HCO_3^- concentrations in the stream waters in October and November (Fig. 3B; Fig. 7B), following the dry summer season, when the discharge began to rise from 107 L·s^{-1} in September to 165 L·s^{-1} in October and to 294 L·s^{-1} in November.

Finally, over the last century, the abandonment of less productive lands in mountainous areas (Chassany, 1999) resulted in the progressive closure of the environment through successive phases of vegetation up to the forest stage (Génot and Schnitzler, 2012; Rameau, 1999). These changes in landscape should have a delayed effect on water chemistry by decreasing discharge and increasing organic matter in soils. The resulting higher production of CO_2 in soils favours the production of carbonic acid and, consequently, the dissolution of minerals leading to an increase of dissolved elements in streamwater. This pattern is being demonstrated in Ulloa-Cedamanos et al.'s (2021).

5. Conclusion

In this study, long-term trends in chemical weathering rates and the associated CO_2 uptake were evaluated based on a unique time data series of major element concentrations and C and S stable isotopes in streamwaters draining a multi-lithological complex karstic catchment. We highlighted that in a multi-lithological complex karst CZ, the different lithological/mineralogical sources could be identified using the distribution of major ions through stoichiometry and statistical methods. Their respective potential contributions to the total stream TDS fluxes as well as their specific weathering rate and CO_2 uptake, were determined by a geochemical discrimination combined with an isotopic approach using novel mixing diagrams based on $\delta^{34}S_{SO4}$ and $\delta^{13}C_{DIC}$ isotopic signatures. The following conclusions can be drawn:

1) Lithology plays an important role on local water chemistry as observed in some silicate-rich (sites B3 and B5) or gypsum-rich (site B8) tributaries in BC. However, in a multilithological context such as in BC, the high solubility of carbonates and their wide distribution lead to a clear dominance on stream TDS compared to other lithologies in the whole catchment.
2) Carbonate dissolution plays a key role in the catchment's carbon sink. The interannual mean weathering rate of carbonates (TZ^+_{carb} + $HCO_{3\_calc./dol.}$, 117 t·Km^{-2}·yr^{-1}) is 11 times higher than that of silicates (TZ^+_{sil}). Chemical weathering pathways are natural and dominated by carbonic acid from atmospheric/soil CO_2, whereas sulphuric acid released by pyrite oxidation takes part in the carbonate dissolution mainly during summer (up to 8.4% of interannual monthly carbonate dissolution).
3) Hydrological conditions, temperature, and epikarst dynamics drive the seasonal variations of riverine TDS fluxes, while the interannual variations are mainly controlled by the discharge. Distribution of the different lithological formations and water dynamic characterise the

spatial variations within the catchment. Besides, landscape changes over the last decades may also have influenced the chemical trends in BC.

4) CO_2 outgassing and calcite precipitation shift the riverine $\delta^{13}C_{DIC}$ signals inherited from the biogenic CO_2 or carbonate dissolution. This could be highlighted by isotopic values from the mixing diagram $\delta^{13}C_{DIC}$–R_{SO4} which displayed a large range of HCO_3^- removal by calcite precipitation at the outlet of BC.
5) A novel $\delta^{34}S_{SO4}$–R_{SO4} mixing diagram was proposed to determine the main weathering pathways in pristine sulphate-rich catchments. The proposed tool revealed a strong sensitivity to detect and to better restrict the potential contribution at sites where sulphate is the dominant anion. Thus, we could demonstrate the potential for $\delta^{34}S_{SO4}$ to be used as a diagnostic tool to help constrain chemical weathering processes in multilithological catchments.
6) The total CO_2 consumption (1595×10^3 mol·km^{-2}·yr^{-1}) by carbonate dissolution and silicate hydrolysis in BC is relatively high compared with other regions in the world, particularly for carbonate dissolution which contributed to 71% of the total CO_2 uptake. On a global scale, the significant relationship between the weathering CO_2 fluxes and the runoff intensity for different regions in the world showed that runoff remains the main driver for CO_2 uptake.

This study opens interesting prospects on the identification and quantification of the geochemical in-stream processes in complex carbonated areas, coupling classical geochemical discrimination (based on stoichiometry calculations) with C and S isotopic signatures. Continuous high-frequency monitoring in time and in space are needed in future works to highlight hot spots and hot moments of weathering processes and CO_2 uptake, and to better model carbon dynamics into the critical zone.

Author contributions

Conceptualization, F.U.-C., A.P. and J.-L.P.; methodology, F.U.-C., A. P. and J.-L.P.; validation, F.U.-C., A.P., J.-L.P.; formal analysis, F.U.-C.; investigation, F.U-C., A.P. and J.-L.P.; resources, F. U-C. and I.M.; data curation, F.U.-C.; writing—original draft preparation, F.U-C.; writing—review and editing, A.P. and J.-L.P.; visualization, F.U.-C.; supervision, A.P. and J.-L.P.; project administration, A.P., J.-L.P.; funding acquisition, A.P., J.-L.P. All authors have read and agreed to the published version of the manuscript.

Funding

This research was supported by the CNRS-INSU within the framework of the SNO Karst and IR OZCAR and by the CNRS-INEE within the framework of the LTSER Zone Atelier Pyrénées-Garonne, which is part of the IR RZA.

Declaration of Competing Interest

The authors declare that they have no known competing financial interests or personal relationships that could have appeared to influence the work reported in this paper.

Acknowledgments

The BC belongs to the French Karst Network (SNO Karst, Jourde et al., 2018; www.sokarst.org) initiative of the INSU/CNRS, which aims to strengthen knowledge-sharing and to promote cross-disciplinary research on karst systems. It is one of the observatories of the French Research Infrastructure called OZCAR (the French network of Critical Zone Observatories, Gaillardet et al., 2018) and also a LTSER (Long-Term Socio-Ecological Reasearch) research site of the CNRS (National Center for Scientific Research) collaborative research platform called "Zone Atelier Pyrénées-Garonne (ZA PYGAR)", which belongs to a French Research Infrastructure called RZA (Réseau des Zones Ateliers, Bretagnolle et al., 2019). RZA grouped with OZCAR is the French contribution to the European Research Infrastructure eLTER (Long-Term Ecosystem in Europe, Mirtl et al., 2018). The authors specially thank the support from CNRS INEE and INSU, SNO KARST, OZCAR and Zone Atelier Pyrénées-Garonne (LTSER ZA PYGAR).

The analytical platforms, PAPC (F. Julien, V. Payre-Suc, D. Lambrigot, and W. Amblas) and SHIVA (I. Moussa and D. Dalger) at Laboratoire écologie fonctionnelle et environnement, and the chemical lab service from the GET (C. Causserand and P. Besson) are thanked for their contribution to the analytical work during the more recent years. F. Ulloa-Cedamanos's PhD was supported by a fellowship from the French Ministry of Higher Education, Research and Innovation. Special thanks are given to Thierry Camboulive, Virginie Payre-Suc, Corinne Pautot, Franck Granouillac, Betty Chaumet and Vanessa Dos-Santos for their help in the field samplings and/or lab works.

Appendix A. Supplementary data

Supplementary data to this article can be found online at https://doi.org/10.1016/j.chemgeo.2021.120567.

References

ADES database, 2021. Point d'eau BSS002MAYC (10734X0010/HY) BAGET [WWW Document]. https://ades.eaufrance.fr/Fiche/PtEau?Code=10734X0010/HY.

Alkattan, M., Oelkers, E.H., Dandurand, J.L., Schott, J., 1998. An experimental study of calcite and limestone dissolution rates as a function of pH from −1 to 3 and temperature from 25 to 80°C. Chem. Geol. 151, 199–214. https://doi.org/10.1016/S0009-2541(98)00080-1.

Amiotte Suchet, P., 1995. Cycle du carbone, érosion chimique des continents et transferts vers les océans. Sci. Géol. Bull. Mém. 97, 3–156.

Amiotte Suchet, P., Probst, J.-L., 1993. Modelling of atmospheric CO2 consumption by chemical weathering of rocks: application to the Garonne, Congo and Amazon basins. Chem. Geol. 107, 205–210. https://doi.org/10.1016/0009-2541(93)90174-H.

Amiotte Suchet, P., Probst, J.L., 1995. Erosion chimique du bassin versant du Congo : variabilité spatio-temporelle des flux de CO2 consommé par altération de la croute continentale. In: Gd bassins fluviaux périatlantiques Congo, Niger, Amaz, pp. 51–68.

Amiotte Suchet, P., Probst, J.-L., 1996. Origines du carbone inorganique dissous dans les eaux de la Garonne. Variations saisonnières et interannuelles. Sci. Géol. 49, 101–126. https://doi.org/10.3406/sgeol.1996.1938.

Amiotte Suchet, P., Probst, J.-L., Ludwig, W., 2003. Worldwide distribution of continental rock lithology: implications for the atmospheric/soil CO2 uptake by continental weathering and alkalinity river transport to the oceans. Glob. Biogeochem. Cycles 17, 1038. https://doi.org/10.1029/2002gb001891.

Amiotte-Suchet, P., Aubert, D., Probst, J.L., Gauthier-Lafaye, F., Probst, A., Andreux, F., Viville, D., 1999. δ13C pattern of dissolved inorganic carbon in a small granitic catchment: the Strengbach case study (Vosges mountains, France). Chem. Geol. 159, 129–145. https://doi.org/10.1016/S0009-2541(99)00037-6.

Aquilina, L., Ladouche, B., Dörfliger, N., 2006. Water storage and transfer in the epikarst of karstic systems during high flow periods. J. Hydrol. 327, 472–485. https://doi.org/10.1016/J.JHYDROL.2005.11.054.

Assaker, A., 2016. Hydrologie et Biogéochimie du Bassin Versant du Fleuve Ibrahim: Un Observatoire du Fonctionnement de la Zone Critique au Liban. University of Toulouse, Toulouse INP, France.

Aucour, A.M., Sheppard, S.M.F., Guyomar, O., Wattelet, J., 1999. Use of 13C to trace origin and cycling of inorganic carbon in the Rhone river system. Chem. Geol. 159, 87–105. https://doi.org/10.1016/S0009-2541(99)00035-2.

Bakalowicz, M., 1979. Contribution de la géochimie des eaux à la connaissance de l'aquifère karstique et de la karstification. University Pierre et Marie Curie, Paris, France.

Bakalowicz, M., 2012. Epikarst. In: Encycl. Caves, pp. 284–288. https://doi.org/10.1016/B978-0-12-383832-2.00038-4.

Berner, R.A., 1997. The Rise of Plants and Their Effect on Weathering and Atmospheric CO2, 276, pp. 544–546.

Berner, R.A., Kothavala, Z., 2001. Geocarb III: a revised model of atmospheric CO2 over phanerozoic time. Am. J. Sci. 301, 182–204. https://doi.org/10.2475/ajs.301.2.182.

Berner, R., Lasaga, A., Garrels, R., 1983. The carbonate-silicate geochemical cycle and its effect on atmospheric carbon dioxide over the past 100 million years. Am. J. Sci. 283, 641–683.

Binet, S., Probst, J.L., Batiot, C., Seidel, J.L., Emblanch, C., Peyraube, N., Charlier, J.-B., Bakalowicz, M., Probst, A., 2020. Global warming and acid atmospheric deposition impacts on carbonate dissolution and CO2 fluxes in French karst hydrosystems: evidence from hydrochemical monitoring in recent decades. Geochim. Cosmochim. Acta 270, 184–200. https://doi.org/10.1016/J.GCA.2019.11.021.

Blum, J.D., Gazis, C.A., Jacobson, A.D., Page Chamberlain, C., 1998. Carbonate versus silicate weathering in the Raikhot watershed within the High Himalayan Crystalline Series. Geology 26, 411–414. https://doi.org/10.1130/0091-7613(1998)026<0411:CVSWIT>2.3.CO;2.

Bluth, G.J.S., Kump, L.R., 1994. Lithologic and climatologic controls of river chemistry. Geochim. Cosmochim. Acta 58, 2341–2359. https://doi.org/10.1016/0016-7037(94)90015-9.

Boano, F., Harvey, J.W., Marion, A., Packman, A.I., Revelli, R., Ridolfi, L., Wörman, A., 2014. Hyporheic flow and transport processes: mechanisms, models, and biogeochemical implications. Rev. Geophys. 52, 603–679. https://doi.org/10.1002/2012RG000417.

Bretagnolle, V., Benoit, M., Bonnefond, M., Breton, V., Church, J.M., Gaba, S., Gilbert, D., Gillet, F., Glatron, S., Guerbois, C., Lamouroux, N., Lebouvier, M., Mazé, C., Mouchel, J.M., Ouin, A., Pays, O., Piscart, C., Ragueneau, O., Servain, S., Spiegelberger, T., Fritz, H., 2019. Action-orientated research and framework: insights from the French longterm social-ecological research network. Ecol. Soc. 24. https://doi.org/10.5751/ES-10989-240310.

Brunet, F., Gaiero, D., Probst, J.L., Depetris, P.J., Lafaye, F.G., Stille, P., 2005. δ13C tracing of dissolved inorganic carbon sources in patagonian rivers (Argentina). Hydrol. Process. 19, 3321–3344. https://doi.org/10.1002/hyp.5973.

Brunet, F., Dubois, K., Veizer, J., Nkoue Ndondo, G.R., Ndam Ngoupayou, J.R., Boeglin, J.L., Probst, J.L., 2009. Terrestrial and fluvial carbon fluxes in a tropical watershed: Nyong basin, Cameroon. Chem. Geol. 265, 563–572. https://doi.org/10.1016/j.chemgeo.2009.05.020.

Brunet, F., Potot, C., Probst, A., Probst, J.L., 2011. Stable Carbon isotope evidence for nitrogenous fertilizer impact on carbonate weathering in a small agricultural watershed. Rapid Commun. Mass Spectrom. 25, 2682–2690. https://doi.org/10.1002/rcm.5050.

Burke, A., Present, T.M., Paris, G., Rae, E.C.M., Sandilands, B.H., Gaillardet, J., Peucker-Ehrenbrink, B., Fischer, W.W., McClelland, J.W., Spencer, R.G.M., Voss, B.M., Adkins, J.F., 2018. Sulphur isotopes in rivers: insights into global weathering budgets, pyrite oxidation, and the modern sulphur cycle. Earth Planet. Sci. Lett. 496, 168–177. https://doi.org/10.1016/j.epsl.2018.05.022.

Busico, G., Kazakis, N., Cuoco, E., Colombani, N., Tedesco, D., Voudouris, K., Mastrocicco, M., 2020. A novel hybrid method of specific vulnerability to anthropogenic pollution using multivariate statistical and regression analyses. Water Res. 171, 115386. https://doi.org/10.1016/j.watres.2019.115386.

Calmels, D., Gaillardet, J., Brenot, A., France-Lanord, C., 2007. Sustained sulphide oxidation by physical erosion processes in the Mackenzie River basin: climatic perspectives. Geology 35, 1003–1006. https://doi.org/10.1130/G24132A.1.

Calmels, D., Gaillardet, J., François, L., 2014. Sensitivity of carbonate weathering to soil CO2 production by biological activity along a temperate climate transect. Chem. Geol. 390, 74–86. https://doi.org/10.1016/j.chemgeo.2014.10.010.

Cao, J., Yuan, D., Groves, C., Huang, F., Yang, H., Lu, Q., 2012. Carbon fluxes and sinks: the consumption of atmospheric and soil CO2 by carbonate rock dissolution. Acta Geol. Sin. 86, 963–972. https://doi.org/10.1111/j.1755-6724.2012.00720.x.

Cao, Y., Xuan, Y., Tang, C., Guan, S., Peng, Y., 2019. Temporary and net sinks of atmospheric CO2 due to chemical weathering in subtropical catchment with mixing carbonate and silicate lithology. Biogeosciences 17, 3875–3890. https://doi.org/10.5194/bg-2019-310.

Catalán, N., Marcé, R., Kothawala, D.N., Tranvik, L.J., 2016. Organic carbon decomposition rates controlled by water retention time across inland waters. Nat. Geosci. 9, 501–504. https://doi.org/10.1038/ngeo2720.

Chassany, J.-P., 1999. Processus de déprise agricole et enjeux socio-économiques. In: Ingénéries - EAT, pp. 81–89.

Chetelat, B., Liu, C.Q., Zhao, Z.Q., Wang, Q.L., Li, S.L., Li, J., Wang, B.L., 2008. Geochemistry of the dissolved load of the Changjiang Basin rivers: anthropogenic impacts and chemical weathering. Geochim. Cosmochim. Acta 72, 4254–4277. https://doi.org/10.1016/j.gca.2008.06.013.

Choukroune, P., 1970. Contribution à l'étude structurale de la zone nordpyrénéenne métamorphique: tectonique et métamorphisme des formations secondaires de la forêt de Boucheville (P.O.). Bull. BRGM 1 (4), 46–63.

Clark, I., Fritz, P., 1997. Environmental Isotopes in Hydrogeology. CRC Press/Lewis Publishers, Boca Raton, FL.

Cloutier, V., Lefebvre, R., Therrien, R., Savard, M.M., 2008. Multivariate statistical analysis of geochemical data as indicative of the hydrogeochemical evolution of groundwater in a sedimentary rock aquifer system. J. Hydrol. 353, 294–313. https://doi.org/10.1016/J.JHYDROL.2008.02.015.

Clow, D.W., Mast, M.A., 2010. Mechanisms for chemostatic behavior in catchments: implications for CO2 consumption by mineral weathering. Chem. Geol. 269, 40–51. https://doi.org/10.1016/J.CHEMGEO.2009.09.014.

Curl, R.L., 2012. Carbon shifted but not sequestered. Science (80-) 335, 655–657. https://doi.org/10.1126/science.335.6069.655-a.

Dalai, T.K., Krishnaswami, S., Sarin, M.M., 2002. Major ion chemistry in the headwaters of the Yamuna river system. Geochim. Cosmochim. Acta 66, 3397–3416. https://doi.org/10.1016/s0016-7037(02)00937-7.

Daoxian, Y., 1997. Sensitivity of karst process to environmental change along the PEP II transect. Quat. Int. 37, 105–113.

Das, A., Krishnaswami, S., Bhattacharya, S.K., 2005. Carbon isotope ratio of dissolved inorganic carbon (DIC) in rivers draining the Deccan Traps, India: sources of DIC and their magnitudes. Earth Planet. Sci. Lett. 236, 419–429. https://doi.org/10.1016/j.epsl.2005.05.009.

Debroas, E., 2009. Géologie du bassin versant du Baget (zone nord-pyrénéenne, Ariège, France) : nouvelles observations et conséquences. Strata 46, 1–93.

Debroas, E.-J., Souquet, P., 1972. Contribution à la connaissance du flysch ardoisier nord-pyrénéen : les "schistes métamorphiques" du synclinal de la Ballongue (Pyrénées centrales). CR Somm. Acad. Sci. Paris II 2813–2816.

Deines, P., 1980. Chapter 9 - the isotopic composition of reduced organic carbon. In: Fritz, P., Fontes, J.C. (Eds.), Handbook of Environmental Isotope Geochemistry. Elsevier, pp. 329–406. https://doi.org/10.1016/b978-0-444-41780-0.50015-8.

Deines, P., Langmuir, D., Harmon, R.S., 1974. Stable carbon isotope ratios and the existence of a gas phase in the evolution of carbonate ground waters. Geochim. Cosmochim. Acta 38, 1147–1164. https://doi.org/10.1016/0016-7037(74)90010-6.

Deirmendjian, L., Abril, G., 2018. Carbon dioxide degassing at the groundwater-stream-atmosphere interface: isotopic equilibration and hydrological mass balance in a sandy watershed. J. Hydrol. 558, 129–143. https://doi.org/10.1016/j.jhydrol.2018.01.003.

Ding, H., Liu, C.Q., Zhao, Z.Q., Li, S.L., Lang, Y.C., Li, X.D., Hu, J., Liu, B.J., 2017. Geochemistry of the dissolved loads of the Liao River basin in northeast China under anthropogenic pressure: chemical weathering and controlling factors. J. Asian Earth Sci. 138, 657–671. https://doi.org/10.1016/j.jseaes.2016.07.026.

Doctor, D.H., Kendall, C., Sebestyen, S.D., Shanley, J.B., Ohte, N., Boyer, E.W., 2008. Carbon isotope fractionation of dissolved inorganic carbon (DIC) due to outgassing of carbon dioxide from a headwater stream. Hydrol. Process. 22, 2410–2423. https://doi.org/10.1002/hyp.

Donnini, M., Frondini, F., Probst, J.-L., Probst, A., Cardellini, C., Marchesini, I., Guzzetti, F., 2016. Chemical weathering and consumption of atmospheric carbon dioxide in the Alpine region. Glob. Planet. Change 136, 65–81. https://doi.org/10.1016/J.GLOPLACHA.2015.10.017.

Eiriksdottir, E.S., Gislason, S.R., Oelkers, E.H., 2011. Does runoff or temperature control chemical weathering rates? Appl. Geochem. 26, S346–S349. https://doi.org/10.1016/j.apgeochem.2011.03.056.

Francois, L.M., Walker, J.C.G., 1992. Modelling the Phanerozoic carbon cycle and climate: constrains from the 87Sr/86Sr isotopic ratio of seawater. Am. J. Sci. 292, 81–135. https://doi.org/10.2475/ajs.292.2.81.

Gaillardet, J., Dupre, B., Louvat, P., Allegre, C.J., 1999. Global silicate weathering and CO2 consumption rates deduced from the chemistry of large rivers. Chem. Geol. 159, 3–30. https://doi.org/10.1016/S0009-2541(99)00031-5.

Gaillardet, J., Braud, I., Hankard, F., Anquetin, S., Bour, O., Dorfliger, N., de Dreuzy, J.R., Galle, S., Galy, C., Gogo, S., Gourcy, L., Habets, F., Laggoun, F., Longuevergne, L., Le Borgne, T., Naaim-Bouvet, F., Nord, G., Simonneaux, V., Six, D., Tallec, T., Valentin, C., Abril, G., Allemand, P., Arènes, A., Arfib, B., Arnaud, L., Arnaud, N., Arnaud, P., Audry, S., Comte, V.B., Batiot, C., Battais, A., Bellot, H., Bernard, E., Bertrand, C., Bessière, H., Binet, S., Bodin, J., Bodin, X., Boithias, L., Bouchez, J., Boudevillain, B., Moussa, I.B., Branger, F., Braun, J.J., Brunet, P., Caceres, B., Calmels, D., Cappelaere, B., Celle-Jeanton, H., Chabaux, F., Chalikakis, K., Champollion, C., Copard, Y., Cotel, C., Davy, P., Deline, P., Delrieu, G., Demarty, J., Dessert, C., Dumont, M., Emblanch, C., Ezzahar, J., Estèves, M., Favier, V., Faucheux, M., Filizola, N., Flammarion, P., Floury, P., Fovet, O., Fournier, M., Francez, A.J., Gandois, L., Gascuel, C., Gayer, E., Genthon, C., Gérard, M.F., Gilbert, D., Gouttevin, I., Grippa, M., Gruau, G., Jardani, A., Jeanneau, L., Join, J.L., Jourde, H., Karbou, F., Labat, D., Lagadeuc, Y., Lajeunesse, E., Lastennet, R., Lavado, W., Lawin, E., Lebel, T., Le Bouteiller, C., Legout, C., Lejeune, Y., Le Meur, E., Le Moigne, N., Lions, J., Lucas, A., Malet, J.P., Marais-Sicre, C., Maréchal, J.C., Marlin, C., Martin, P., Martins, J., Martinez, J.M., Massei, N., Mauclerc, A., Mazzilli, N., Molénat, J., Moreira-Turcq, P., Mougin, E., Morin, S., Ngoupayou, J.N., Panthou, G., Peugeot, C., Picard, G., Pierret, M.C., Porel, G., Probst, A., Probst, J.L., Rabatel, A., Raclot, D., Ravanel, L., Rejiba, F., René, P., Ribolzi, O., Riotte, J., Rivière, A., Robain, H., Ruiz, L., Sanchez-Perez, J.M., Santini, W., Sauvage, S., Schoeneich, P., Seidel, J.L., Sekhar, M., Sengtaheuanghoung, O., Silvera, N., Steinmann, M., Soruco, A., Tallec, G., Thibert, E., Lao, D.V., Vincent, C., Viville, D., Wagnon, P., Zitouna, R., 2018. OZCAR: the French network of critical zone observatories. Vadose Zo J. 17, 1–24. https://doi.org/10.2136/vzj2018.04.0067.

Gaillardet, J., Calmels, D., Romero-Mujalli, G., Zakharova, E., Hartmann, J., 2019. Global climate control on carbonate weathering intensity. Chem. Geol. 527, 118762. https://doi.org/10.1016/j.chemgeo.2018.05.009.

Galy, A., France-Lanord, C., 1999. Weathering processes in the Ganges-Brahmaputra basin and the riverine alkalinity budget. Chem. Geol. 159, 31–60. https://doi.org/10.1016/S0009-2541(99)00033-9.

Gao, Q., Tao, Z., Huang, X., Nan, L., Yu, K., Wang, Z., 2009. Chemical weathering and CO2 consumption in the Xijiang River basin, South China. Geomorphology 106, 324–332. https://doi.org/10.1016/j.geomorph.2008.11.010.

Garrels, R.M., MacKenzie, F.T., 1972. A quantitative model for the sedimentary rock cycle. Mar. Chem. 1, 27–41. https://doi.org/10.1016/0304-4203(72)90004-7.

Génot, J.-C., Schnitzler, A., 2012. La France des friches. De la ruralité à la féralité. Matière à débattre et décider, Éditions Quæ, Versailles.

Gibbs, R.J., 1972. Water chemistry of the Amazon River. Geochim. Cosmochim. Acta 36, 1061–1066. https://doi.org/10.1016/0016-7037(72)90021-X.

Gislason, S.R., Oelkers, E.H., Eiriksdottir, E.S., Kardjilov, M.I., Gisladottir, G., Sigfusson, B., Snorrason, A., Elefsen, S., Hardardottir, J., Torssander, P., Oskarsson, N., 2009. Direct evidence of the feedback between climate and weathering. Earth Planet. Sci. Lett. 277, 213–222. https://doi.org/10.1016/j.epsl.2008.10.018.

Goudie, A.S., Viles, H.A., 2012. Weathering and the global carbon cycle: geomorphological perspectives. Earth Sci. Rev. 113, 59–71. https://doi.org/10.1016/j.earscirev.2012.03.005.

Hagedorn, B., Cartwright, I., 2009. Climatic and lithologic controls on the temporal and spatial variability of CO2 consumption via chemical weathering: an example from

the Australian Victorian Alps. Chem. Geol. 260, 234–253. https://doi.org/10.1016/j.chemgeo.2008.12.019.
Hamilton, N., 2018. ggtern: An Extension to 'ggplot2', for the Creation of Ternary Diagrams. R Package Version 2.2.2.
Han, G., Liu, C.Q., 2004. Water geochemistry controlled by carbonate dissolution: a study of the river waters draining karst-dominated terrain, Guizhou Province, China. Chem. Geol. 204, 1–21. https://doi.org/10.1016/j.chemgeo.2003.09.009.
Hartmann, J., Jansen, N., Dürr, H.H., Kempe, S., Köhler, P., 2009. Global CO2-consumption by chemical weathering: what is the contribution of highly active weathering regions? Glob. Planet. Change 69, 185–194. https://doi.org/10.1016/j.gloplacha.2009.07.007.
Hem, J.D., 1986. Study and interpretation of the chemical characteristics of natural water. In: U.S. Geol. Survey Water-Supply Paper 2254, Third ed.
Hercod, D.J., Brady, P.V., Gregory, R.T., 1998. Catchment-scale coupling between pyrite oxidation and calcite weathering. Chem. Geol. 151, 259–276. https://doi.org/10.1016/S0009-2541(98)00084-9.
Hounslow, A.W., 1995. Water Quality Data: Analysis and Interpretation. CRC Press.
Huh, Y., Tsoi, M.Y., Zaitsev, A., Edmond, J.M., 1998. The fluvial geochemistry of the rivers of eastern Siberia: I. Tributaries of the Lena River draining the sedimentary platform of the Siberian Craton. Geochim. Cosmochim. Acta 62, 1657–1676. https://doi.org/10.1016/S0016-7037(98)00107-0.
Jacobson, A.D., Blum, J.D., Chamberlain, C.P., Craw, D., Koons, P.O., 2003. Climatic and tectonic controls on chemical weathering in the New Zealand Southern Alps. Geochim. Cosmochim. Acta 67, 29–46. https://doi.org/10.1016/S0016-7037(02)01053-0.
Jiang, Y., 2012. Sources of sulphur in the Nandong underground river system, southwest China: a chemical and isotopic reconnaissance. Appl. Geochem. 27, 1463–1470. https://doi.org/10.1016/j.apgeochem.2012.05.001.
Jiang, H., Liu, W., Xu, Z., Zhou, X., Zheng, Z., Zhao, T., Zhou, L., Zhang, X., Xu, Y., Liu, T., 2018. Chemical weathering of small catchments on the Southeastern Tibetan Plateau I: water sources, solute sources and weathering rates. Chem. Geol. 500, 159–174. https://doi.org/10.1016/j.chemgeo.2018.09.030.
Jourde, H., Massei, N., Mazzilli, N., Binet, S., Batiot-Guilhe, C., Labat, D., Steinmann, M., Bailly-Comte, V., Seidel, J.L., Arfib, B., Charlier, J.B., Guinot, V., Jardani, A., Fournier, M., Aliouache, M., Babic, M., Bertrand, C., Brunet, P., Boyer, J.F., Bricquet, J.P., Camboulive, T., Carrière, S.D., Celle-Jeanton, H., Chalikakis, K., Chen, N., Cholet, C., Clauzon, V., Dal Soglio, L., Danquigny, C., Défargue, C., Denimal, S., Emblanch, C., Hernandez, F., Gillon, M., Gutierrez, A., Hidalgo Sanchez, L., Hery, M., Houillon, N., Johannet, A., Jouves, J., Jozja, N., Ladouche, B., Leonardi, V., Lorette, G., Loup, C., Marchand, P., de Montety, V., Muller, R., Ollivier, C., Sivelle, V., Lastennet, R., Lecoq, N., Maréchal, J.C., Perotin, L., Perrin, J., Petre, M.A., Peyraube, N., Pistre, S., Plagnes, V., Probst, A., Probst, J.-L., Simler, R., Stefani, V., Valdes-Lao, D., Viseur, S., Wang, X., 2018. SNO KARST: a french network of observatories for the multidisciplinary study of critical zone processes in karst watersheds and aquifers. Vadose Zo J. 17 https://doi.org/10.2136/vzj2018.04.0094.
Karim, A., Veizer, J., 2000. Weathering processes in the Indus River Basin: implications from riverine carbon, sulphur, oxygen, and strontium isotopes. Chem. Geol. 170, 153–177. https://doi.org/10.1016/S0009-2541(99)00246-6.
Kemeny, P.C., Lopez, G.I., Dalleska, N.F., Torres, M., Burke, A., Bhatt, M.P., West, A.J., Hartmann, J., Adkins, J.F., 2021. Sulphate sulphur isotopes and major ion chemistry reveal that pyrite oxidation counteracts CO2 drawdown from silicate weathering in the Langtang-Trisuli-Narayani River system, Nepal Himalaya. Geochim. Cosmochim. Acta 294, 43–69. https://doi.org/10.1016/j.gca.2020.11.009.
Khadka, M.B., Martin, J.B., Jin, J., 2014. Transport of dissolved carbon and CO2 degassing from a river system in a mixed silicate and carbonate catchment. J. Hydrol. 513, 391–402. https://doi.org/10.1016/j.jhydrol.2014.03.070.
Kirchner, J.W., 2003. A double paradox in catchment hydrology and geochemistry. Hydrol. Process. 17, 871–874. https://doi.org/10.1002/hyp.5108.
Lang, Y.C., Liu, C.Q., Li, S.L., Zhao, Z.Q., Zhou, Z.H., 2011. Tracing natural and anthropogenic sources of dissolved sulphate in a karst region by using major ion chemistry and stable sulphur isotopes. Appl. Geochem. 26, S202–S205. https://doi.org/10.1016/j.apgeochem.2011.03.104.
Lechuga-Crespo, J.L., Ruiz-Romera, E., Probst, J.L., Unda-Calvo, J., Cuervo-Fuentes, Z.C., Sánchez-Pérez, J.M., 2020. Combining punctual and high frequency data for the spatiotemporal assessment of main geochemical processes and dissolved exports in an urban river catchment. Sci. Total Environ. 727, 138644. https://doi.org/10.1016/j.scitotenv.2020.138644.
Lenton, T.M., Britton, C., 2006. Enhanced carbonate and silicate weathering accelerates recovery from fossil fuel CO2 perturbations. Glob. Biogeochem. Cycles 20, 1–12. https://doi.org/10.1029/2005GB002678.
Li, S.L., Calmels, D., Han, G., Gaillardet, J., Liu, C.Q., 2008. Sulphuric acid as an agent of carbonate weathering constrained by δ13CDIC: examples from Southwest China. Earth Planet. Sci. Lett. 270, 189–199. https://doi.org/10.1016/j.epsl.2008.02.039.
Li, S.-L., Liu, C.-Q., Li, J., Lang, Y.-C., Ding, H., Li, L., 2010. Geochemistry of dissolved inorganic carbon and carbonate weathering in a small typical karstic catchment of Southwest China: isotopic and chemical constrains. Chem. Geol. 277, 301–309. https://doi.org/10.1016/J.CHEMGEO.2010.08.013.
Liu, J., Han, G., 2020a. Effects of chemical weathering and CO2 outgassing on δ13CDIC signals in a karst watershed. J. Hydrol. 589, 125192. https://doi.org/10.1016/j.jhydrol.2020.125192.
Liu, J., Han, G., 2020b. Major ions and δ34SSO4 in Jiulongjiang River water: investigating the relationships between natural chemical weathering and human perturbations. Sci. Total Environ. 724, 138208. https://doi.org/10.1016/j.scitotenv.2020.138208.
Liu, Z., Zhao, J., 2000. Contribution of carbonate rock weathering to the atmospheric CO2 sink. Environ. Geol. 39, 1053–1058.
Liu, B., Liu, C.Q., Zhang, G., Zhao, Z.Q., Li, S.L., Hu, J., Ding, H., Lang, Y.C., Li, X.D., 2013. Chemical weathering under mid- to cool temperate and monsoon-controlled climate: a study on water geochemistry of the Songhuajiang River system, northeast China. Appl. Geochem. 31, 265–278. https://doi.org/10.1016/j.apgeochem.2013.01.015.
Liu, Z., Macpherson, G.L., Groves, C., Martin, J.B., Yuan, D., Zeng, S., 2018. Large and active CO2 uptake by coupled carbonate weathering. Earth Sci. Rev. 182, 42–49. https://doi.org/10.1016/J.EARSCIREV.2018.05.007.
Lucas, Y., 2001. The role of plants in controlling rates and products of weathering: importance of biological pumping. Annu. Rev. Earth Planet. Sci. 29, 135–163. https://doi.org/10.1146/annurev.earth.29.1.135.
Macpherson, G.L., Sullivan, P.L., 2019. Watershed-scale chemical weathering in a merokarst terrain, northeastern Kansas, USA. Chem. Geol. 527, 118988. https://doi.org/10.1016/j.chemgeo.2018.12.001.
Maher, K., Chamberlain, C.P., 2014. Hydrologic regulation of chemical weathering and the geologic. Science (80-) 343, 1502–1504. https://doi.org/10.1126/science.1250770.
Mangin, A., 1975. Contribution à l'étude hydrodynamique des aquifères karstiques (Ann. Spéléo., 1974 29: 283-332; 1974 29: 495-601; 1975 30: 21-124). Université de Dijon, Dijon, France.
Mangin, A., 1984. Pour une meilleure connaissance des systèmes hydrologiques à partir des analyses corrélatoire et spectrale. J. Hydrol. 67, 25–43. https://doi.org/10.1016/0022-1694(84)90230-0.
Marx, A., Dusek, J., Jankovec, J., Sanda, M., Vogel, T., van Geldern, R., Hartmann, J., Barth, J.A.C., 2017. A review of CO2 and associated carbon dynamics in headwater streams: a global perspective. Rev. Geophys. 55, 560–585. https://doi.org/10.1002/2016RG000547.
Meybeck, M., 1986. Composition chimique des ruisseaux non pollués en France. Chemical composition of headwater streams in France. Sci. Géol. 39, 3–77. https://doi.org/10.3406/sgeol.1986.1719.
Meybeck, M., 1987. Global chemical weathering of surficial rocks estimated from river dissolved loads. Am. J. Sci. 287, 401–428.
Meybeck, M., 2003. Global Occurrence of Major Elements in Rivers, Treatise on Geochemistry. Pergamon. https://doi.org/10.1016/B0-08-043751-6/05164-1.
Millot, R., Gaillardet, J., Dupré, B., Allégre, C.J., 2003. Northern latitude chemical weathering rates: clues from the Mackenzie River Basin, Canada. Geochim. Cosmochim. Acta 67, 1305–1329. https://doi.org/10.1016/S0016-7037(02)01207-3.
Mirtl, M.T., Borer, E., Djukic, I., Forsius, M., Haubold, H., Hugo, W., Jourdan, J., Lindenmayer, D., McDowell, W.H., Muraoka, H., Orenstein, D.E., Pauw, J.C., Peterseil, J., Shibata, H., Wohner, C., Yu, X., Haase, P., 2018. Genesis, goals and achievements of Long-Term Ecological Research at the global scale: A critical review of ILTER and future directions. Sci. Total Environ. 626, 1439–1462. https://doi.org/10.1016/j.scitotenv.2017.12.001.
Mook, W.G., 2000. Volume I. Introduction, theory, methods, review. In: Environmental Isotopes in the Hydrological Cycle : Principles and Applications. Technical Documents in Hydrology, N° 39. UNESCO/ IAEA, Paris, pp. 1–170.
Moon, S., Huh, Y., Qin, J., van Pho, N., 2007. Chemical weathering in the Hong (Red) River basin: rates of silicate weathering and their controlling factors. Geochim. Cosmochim. Acta 71, 1411–1430. https://doi.org/10.1016/j.gca.2006.12.004.
Moquet, J.S., Crave, A., Viers, J., Seyler, P., Armijos, E., Bourrel, L., Chavarri, E., Lagane, C., Laraque, A., Sven, W., Casimiro, L., Pombosa, R., Noriega, L., Vera, A., Guyot, J.L., 2011. Chemical weathering and atmospheric / soil CO2 uptake in the Andean and Foreland Amazon basins. Chem. Geol. 287, 1–26. https://doi.org/10.1016/j.chemgeo.2011.01.005.
Moquet, J.S., Guyot, J.L., Crave, A., Viers, J., Filizola, N., Martinez, J.M., Oliveira, T.C., Sánchez, L.S.H., Lagane, C., Casimiro, W.S.L., Noriega, L., Pombosa, R., 2016. Amazon River dissolved load: temporal dynamics and annual budget from the Andes to the ocean. Environ. Sci. Pollut. Res. 23, 11405–11429. https://doi.org/10.1007/s11356-015-5503-6.
Mortatti, J., Probst, J.-L., 2003. Silicate rock weathering and atmospheric/soil CO2 uptake in the Amazon basin estimated from river water geochemistry: seasonal and spatial variations. Chem. Geol. 197, 177–196. https://doi.org/10.1016/S0009-2541(02)00349-2.
Parkhurst, D.L., Appelo, C.A.J., 1999. User's Guide to PHREEQC (Version 2): A Computer Program for Speciation, Batch-reaction, One-dimensional Transport, and Inverse Geochemical Calculations. U.S. Geological Survey, Denver, Colorado.
Peyraube, N., Lastennet, R., Denis, A., Malaurent, P., 2013. Estimation of epikarst air PCO2 using measurements of water δ13CTDIC, cave air PCO2 and δ13CCO2. Geochim. Cosmochim. Acta 118, 1–17. https://doi.org/10.1016/J.GCA.2013.03.046.
Pierret, M.C., Viville, D., Dambrine, E., Cotel, S., Probst, A., 2019. Twenty-five year record of chemicals in open field precipitation and throughfall from a medium-altitude forest catchment (Strengbach - NE France): an obvious response to atmospheric pollution trends. Atmos. Environ. 202, 296–314. https://doi.org/10.1016/j.atmosenv.2018.12.026.
Piper, A., 1944. A graphic procedure in geochemical interpretation of water analyses. Trans. Am. Geophys. Union 25, 914–923.
Plan, L., Decker, K., Faber, R., Wagreich, M., Grasemann, B., 2009. Karst morphology and groundwater vulnerability of high alpine karst plateaus. Environ. Geol. 58, 285–297. https://doi.org/10.1007/s00254-008-1605-5.
Plummer, L., Busenberg, E., 1982. The solubilities of calcite, aragonite and vaterite in CO2-H2O solutions between 0 and 90°C, and an evaluation of the aqueous model for

the system CaCO3-CO2-H2O. Geochim. Cosmochim. 46, 1011–1040. https://doi.org/10.1016/0016-7037(82)90056-4.
Porcal, P., Dillon, P.J., Molot, L.A., 2015. Temperature dependence of photodegradation of dissolved organic matter to dissolved inorganic carbon and particulate organic carbon. PLoS One 10, 1–15. https://doi.org/10.1371/journal.pone.0128884.
Probst, J.-L., 1992. Géochimie et hydrologie de l'érosion continentale. Mécanismes, bilan global actuel et fluctuations au cours des 500 derniers millions d'années. Sci. Géol. Mém. 94, 3–164.
Probst, A., Viville, D., Fritz, B., Ambroise, B., Dambrine, E., 1992. Hydrochemical budgets of a small forested granitic catchment exposed to acid deposition: the strengbach catchment case study (Vosges massif, France). Water Air Soil Pollut. 62, 337–347. https://doi.org/10.1007/BF00480265.
Probst, J.-L., Ludwig, W., Amiotte Suchet, P., 1997. Global modeling of CO2 uptake by continental erosion and of carbon river transport to the oceans. Sci. Géol. 50, 131–156. https://doi.org/10.3406/sgeol.1997.1950.
Qibo, H., Xiaoqun, Q., Qiyong, Y., Pengyu, L., Jinsong, Z., 2016. Identification of dissolved sulphate sources and the role of sulphuric acid in carbonate weathering using δ13CDIC and δ34S in karst area, northern China. Environ. Earth Sci. 75, 1–10. https://doi.org/10.1007/s12665-015-4869-6.
Qin, C., Li, S.L., Yue, F.J., Xu, S., Ding, H., 2019. Spatiotemporal variations of dissolved inorganic carbon and controlling factors in a small karstic catchment, Southwestern China. Earth Surf. Proc. Landforms 44, 2423–2436. https://doi.org/10.1002/esp.4672.
Qin, C., Li, S.-L., Waldron, S., Yue, F.-J., Wang, Z.-J., Zhong, J., Ding, H., Liu, C.-Q., 2020. High-frequency monitoring reveals how hydrochemistry and dissolved carbon respond to rainstorms at a karstic critical zone, Southwestern China. Sci. Total Environ. 714, 136833. https://doi.org/10.1016/J.SCITOTENV.2020.136833.
Rameau, J.-C., 1999. Accrus, successions végétales et modèles de dynamique linéaire forestière. In: Ingénieries-EAT, pp. 33–48.
Richey, J.E., Melack, J.M., Aufdenkampe, A.K., Ballester, V.M., Hess, L.L., 2002. Outgassing from Amazonian rivers and wetlands as a large tropical source of atmospheric CO2. Nature 416, 617–620. https://doi.org/10.1038/416617a.
Schöpp, W., Posch, M., Mylona, S., Johansson, M., 2003. Long-term development of acid deposition (1880–2030) in sensitive freshwater regions in Europe. Hydrol. Earth Syst. Sci. 7, 436–446. https://doi.org/10.5194/hess-7-436-2003.
Schulte, P., van Geldern, R., Freitag, H., Karim, A., Négrel, P., Petelet-Giraud, E., Probst, A., Probst, J.-L.L., Telmer, K., Veizer, J., Barth, J.A.C., 2011. Applications of stable water and carbon isotopes in watershed research: weathering, carbon cycling, and water balances. Earth Sci. Rev. 109, 20–31. https://doi.org/10.1016/j.earscirev.2011.07.003.
Singer, P.C., Stumm, W., 1970. Acidic mine drainage: the rate-determining step. Science (80-) 167, 1121–1123. https://doi.org/10.1126/science.167.3921.1121.
Sivelle, V., Labat, D., Mazzilli, N., Massei, N., Jourde, H., 2019. Dynamics of the flow exchanges between matrix and conduits in Karstified watersheds at multiple temporal scales. Water (Switzerland) 11, 1–15. https://doi.org/10.3390/w11030569.
Spence, J., Telmer, K., 2005. The role of sulphur in chemical weathering and atmospheric CO2 fluxes: evidence from major ions, δ13CDIC, and δ34SSO4 in rivers of the Canadian Cordillera. Geochim. Cosmochim. Acta 69, 5441–5458. https://doi.org/10.1016/j.gca.2005.07.011.
Stallard, R.F., Edmond, J.M., 1983. Geochemistry of the Amazon: 2. The influence of geology and weathering environment on the dissolved load. J. Geophys. Res. Ocean 88, 9671–9688. https://doi.org/10.1029/JC088iC14p09671.
Stallard, R.F., Edmond, J.M., 1987. Geochemistry of the Amazon 3. Weathering chemistry and limits to dissolved inputs. J. Geophys. Res. 92, 8293–8302.
Stiff, H.A., 1951. The interpretation of chemical water analysis by means of patterns. J. Pet. Technol. 3, 15–23. https://doi.org/10.2118/951376-g.
Tipper, E.T., Bickle, M.J., Galy, A., West, A.J., Pomiès, C., Chapman, H.J., 2006. The short term climatic sensitivity of carbonate and silicate weathering fluxes: insight from seasonal variations in river chemistry. Geochim. Cosmochim. Acta 70, 2737–2754. https://doi.org/10.1016/J.GCA.2006.03.005.
Turchyn, A.V., Tipper, E.T., Galy, A., Lo, J.K., Bickle, M.J., 2013. Isotope evidence for secondary sulphide precipitation along the Marsyandi River, Nepal, Himalayas. Earth Planet. Sci. Lett. 374, 36–46. https://doi.org/10.1016/j.epsl.2013.04.033.
Ulloa-Cedamanos, F., Probst, J.L., Binet, S., Camboulive, T., Payre-Suc, V., Pautot, C., Bakalowicz, M., Beranger, S., Probst, A., 2020. A forty-year karstic critical zone survey (baget catchment, pyrenees-france): lithologic and hydroclimatic controls on seasonal and inter- annual variations of stream water chemical composition, pCO2, and carbonate equilibrium. Water 12. https://doi.org/10.3390/W12051227.
Ulloa-Cedamanos, F., Probst, A., Dos-Santos, V., Camboulive, T., Granouillac, F., Probst, J.-L., 2021. Stream hydrochemical response to flood events in a multi-lithological karstic catchment from the Pyrenees Mountains (SW France). Water 13, 1818. https://doi.org/10.3390/w13131818.
Veizer, J., Ala, D., Karem, A., Bruckschen, P., 1999. 87Sr/86Sr, d13C and d18O evolution of Phanerozoic seawater. Chem. Geol. 161, 59–88.
Viers, J., Oliva, P., Dandurand, J., Dupre, B., Gaillardet, J., 2014. Chemical weathering rates, CO2 consumption, and control parameters deduced from the chemical composition of rivers. In: Holland, H.D., Turekian, K.K. (Eds.), Treatise on Geochemistry, Second edition. Elsevier, pp. 175–194. https://doi.org/10.1016/B978-0-08-095975-7.00506-4.
Wang, W., Li, S.L., Zhong, J., Li, C., Yi, Y., Chen, S., Ren, Y., 2019. Understanding transport and transformation of dissolved inorganic carbon (DIC)in the reservoir system using δ13CDIC and water chemistry. J. Hydrol. 574, 193–201. https://doi.org/10.1016/j.jhydrol.2019.04.036.
Wang, W.F., Li, S.L., Zhong, J., Maberly, S.C., Li, C., Wang, F.S., Xiao, H.Y., Liu, C.Q., 2020. Climatic and anthropogenic regulation of carbon transport and transformation in a karst river-reservoir system. Sci. Total Environ. 707, 135628. https://doi.org/10.1016/j.scitotenv.2019.135628.
West, A.J., 2012. Thickness of the chemical weathering zone and implications for erosional and climatic drivers of weathering and for carbon-cycle feedbacks. Geology 40, 811–814. https://doi.org/10.1130/G33041.1.
West, A.J., Galy, A., Bickle, M., 2005. Tectonic and climatic controls on silicate weathering. Earth Planet. Sci. Lett. 235, 211–228. https://doi.org/10.1016/j.epsl.2005.03.020.
White, A.F., Blum, A.E., 1995. Effects of climate on chemical weathering in watersheds. In: Water-rock Interact Proc Symp Vladivostok, 1995, 59, pp. 57–60.
Xu, Z., Liu, C.Q., 2007. Chemical weathering in the upper reaches of Xijiang River draining the Yunnan-Guizhou Plateau, Southwest China. Chem. Geol. 239, 83–95. https://doi.org/10.1016/j.chemgeo.2006.12.008.
Zeng, S., Liu, Z., Goldscheider, N., Frank, S., Goeppert, N., Kaufmann, G., Zeng, C., Zeng, Q., Sun, H., 2021. Comparisons on the effects of temperature, runoff, and land-cover on carbonate weathering in different karst catchments: insights into the future global carbon cycle. Hydrogeol. J. 29, 331–345. https://doi.org/10.1007/s10040-020-02252-5.
Zhang, J., Huang, W.W., Létolle, R., Jusserand, C., 1995. Major element chemistry of the Huanghe (Yellow River), China - weathering processes and chemical fluxes. J. Hydrol. 168, 173–203. https://doi.org/10.1016/0022-1694(94)02635-O.
Zhao, R., Liu, Z., Huang, H., Dong, L., 2019. Difference in the relationship between soil - CO2 concentration and the karst - related carbon cycle under different land use types in southwest China. Carbonates Evaporites 34, 1569–1581. https://doi.org/10.1007/s13146-019-00506-2.
Zhong, J., Li, S.L., Tao, F., Yue, F., Liu, C.Q., 2017. Sensitivity of chemical weathering and dissolved carbon dynamics to hydrological conditions in a typical karst river. Sci. Rep. 7, 1–9. https://doi.org/10.1038/srep42944.